

Neglecting model parametric uncertainty can drastically underestimate flood risks

Sanjib Sharma¹, Benjamin Seiyon Lee², Iman Hosseini-Shakib¹, Murali Haran³,
and Klaus Keller⁴

¹Earth and Environmental Systems Institute, Pennsylvania State University, University Park, PA, USA

²Department of Statistics, George Mason University, Fairfax, VA, USA

³Department of Statistics, Pennsylvania State University, University Park, PA, USA

⁴Thayer School of Engineering at Dartmouth College, Hanover, NH, USA

Corresponding author: Sanjib Sharma (svs6308@psu.edu)

Key points:

- We implement a sequential Monte Carlo particle-based Fast Model Calibrations (FaMoS) approach to improve the characterization of distributed hydrologic model parameters.
- FaMos demonstrates a relatively higher prediction skill than stepwise line search and precalibration.
- Accounting for model parametric uncertainty improves the projections of flood damage.

Abstract

Floods drive dynamic and deeply uncertain risks for people and infrastructures. Uncertainty characterization is a crucial step in improving the predictive understanding of multi-sector dynamics and the design of risk-management strategies. Current approaches to estimate flood hazards often sample only a relatively small subset of the known unknowns, for example the uncertainties surrounding the model parameters. This approach neglects the impacts of key uncertainties on hazards and system dynamics. Here we mainstream a recently developed method for Bayesian inference to calibrate a computationally expensive distributed hydrologic model. We compare three different calibration approaches: (1) stepwise line search, (2) precalibration or screening, and (3) the new Fast Model Calibrations (FaMoS) approach. FaMoS deploys a particle-based approach that takes advantage of the massive parallelization afforded by modern high-performance computing systems. We quantify how neglecting parametric uncertainty and data discrepancy can drastically underestimate extreme flood events and risks. Precalibration improves prediction skill score over a stepwise line search. The Bayesian calibration improves the uncertainty characterization of model parameters and flood risk projections.

39 **1. Motivation and Introduction**

40 Floods pose major risks to people and property (Alfieri et al., 2017; Wing et al., 2018;
41 Winsemius et al., 2015). These risks are dynamic and deeply uncertain (Merz et al., 2010; Read &
42 Vogel, 2015; Ruckert et al., 2019; Zarekarizi et al., 2020). It is important to characterize the
43 uncertainties surrounding flood hazards in order to understand the impacts on multi-sector
44 dynamics and to inform the design of risk-management strategies (Boulangé et al., 2021; Chester
45 et al., 2020; Liu & Merwade, 2018; Salas et al., 2018b; Wasko et al., 2021; Wong & Keller, 2017).

46 Hydrologic models are commonly used to understand hydrological processes, predict the
47 response of hydrological systems to changing stresses, and provide boundary conditions to
48 estimate flood hazards and risks (Bates et al., 2021; Brunner et al., 2020; Judi et al., 2018; Koren
49 et al., 2004; Rajib et al., 2020; Thorstensen et al., 2016). However, hydrologic projections are
50 subject to uncertainties such as from model structures, parameters and forcings (Gupta et al., 2012;
51 Kavetski et al., 2006; Beven, 2014; Fisher & Koven, 2020; Hu et al., 2019; Mendoza et al., 2015).
52 Parametric uncertainty can arise, for example, from the epistemic uncertainties about model
53 parameters (Vrugt et al., 2003), the associated prior distributions (Tang et al., 2016), spatial-
54 resolutions and objective functions (Melsen et al., 2019), and different choices of calibration
55 approaches (Kavetski et al., 2018). Hydrologic models need to resolve the complex response of
56 multiple processes (e.g., land surface characteristics, soil properties and climate variability) with
57 strong nonlinear interactions and often few observations. Characterizing parametric uncertainty
58 can be critical to improve prediction credibility and inform decision-making, for example, in the
59 context of water-resources planning and flood-risk management (Herman et al., 2013; Ruckert et
60 al., 2019; Wong & Keller, 2017; Zarekarizi et al., 2020).

61 Previous studies provide valuable new insights on flood hazard and risk estimates using model
62 simulations (Bates et al., 2021; Judi et al., 2018; Rajib et al., 2020; Sanders et al., 2020; Sharma et
63 al., 2021; Wing et al., 2018). For example, Judi et al. (2018) demonstrates an integrated multimodel
64 multiscale simulation approach to evaluate social, economic, and infrastructure resilience to future
65 flooding. Rajib et al. (2020) develops a coupled land surface hydrologic and river hydraulic
66 modeling framework to provide regional flood hazard and risk estimates. Bates et al. (2021)
67 presents estimates of current and future flood risk for all properties in the conterminous United
68 States using a combined modeling approach considering river, coastal, or rainfall flooding. These
69 studies typically obtain an optimal parameter set that produces the best possible agreement

70 between simulated and observed streamflow hydrographs at target locations. These previous
71 studies break important new ground, but are mostly silent on the impacts of parametric
72 uncertainties on hazards and dynamics. Neglecting parametric uncertainties can underestimate the
73 tails of flood hazard probability distribution (Bates et al., 2021; Mendoza et al., 2015; Rojas et al.,
74 2020; Salas et al., 2018a), and can result in poor decisions and outcomes (Ruckert et al., 2019;
75 Wong & Keller, 2017; Zarekarizi et al., 2020).

76 Several studies on hydrologic model calibration have focused on manually adjusting a
77 subset of model parameters (Bitew & Gebremichael, 2011; Siddique & Mejia, 2017). These
78 manual calibrations typically rely on visual inspection of streamflow hydrograph and a trial and
79 error-based procedure; hence, this method can be rather labor-intensive and time-consuming
80 (Lahmers et al., 2021; Siddique & Mejia, 2017). A conceptual intuitive and relatively simple to
81 implement approach for uncertainty characterization is the Generalized Likelihood Uncertainty
82 Estimation (GLUE) method (Beven and Binley, 1992). The GLUE method has many advantages
83 and can provide very useful insights, but several studies point to potential improvements with
84 regard to subjective decisions on the likelihood function and implementing a statistically consistent
85 error model (Blasone et al., 2008; Stedinger et al., 2008). A more complex approach adopted in
86 this area is automatic parameter optimization (Kamali et al., 2013; Van Liew et al., 2005).
87 Automatic calibration relies on systematic search approaches to find the best parameter values
88 based on predefined single- and/or multi-objective functions (Kamali et al., 2013). Some studies
89 use surrogate methods such as Gaussian process-based emulators to help identify best-fit
90 parameters (Gou et al., 2020; Pianosi et al., 2016; Razavi & Tolson, 2013). Gou et al. (2020)
91 presents an automatic calibration framework that combines sensitivity analysis and surrogate-
92 based optimization for calibrating catchment-specific hydrologic model parameters. Surrogate-
93 based methods are typically limited to cases with relatively fewer model parameters because
94 training a surrogate model can be computationally prohibitive with high-dimensional inputs due
95 to the large number of training data required (Hwang & Martins, 2018; Lee et al., 2020; Liu &
96 Guillas, 2017) or repeated evaluations of the gradient of the model output with respect to the input
97 parameters (Constantine et al., 2014; Lataniotis et al., 2020).

98 Bayesian calibration of hydrologic models have become increasingly popular (Hsu et al.,
99 2009; Jeremiah et al., 2011; Kavetski et al., 2018; Raje & Krishnan, 2012; Razavi & Tolson, 2013;
100 Shafii et al., 2015; Su et al., 2018; Zhu et al., 2018). For example, Vrugt et al., (2008) employ an

101 adaptive Metropolis Markov chain Monte Carlo (MCMC) sampling scheme-Differential
102 Evolution Adaptive Metropolis (DREAM) algorithm to explore the entire parameter space of a
103 hydrologic model. Different variants of DREAM algorithm (Vrugt et al., 2008; Vrugt et al., 2009;
104 Laloy and Vrugt, 2012) demonstrate the value of Bayesian approaches on model calibration.
105 Jeremiah et al. (2011) demonstrates an improved efficiency of Sequential Monte Carlo approach
106 over the Adaptive Metropolis MCMC samplers in exploring the parameter space where the optimal
107 solutions lie in the tails of the prescribed prior distribution. Su et al. (2018) uses a Bayesian
108 hierarchical model to calibrate the Priestly–Taylor Jet Propulsion Laboratory model using
109 observed evapotranspiration measurements. Given the relatively short model run times, the
110 hierarchical model can be fit using the Differential Evolution Markov Chain (Braak, 2006; Storn
111 & Price, 1997), a population MCMC algorithm. Zhu et al. (2018) calibrates eight parameters of a
112 conceptual water balance model using a Particle Evolution Metropolis Sequential Monte Carlo
113 (PEM-SMC). The PEM-SMC algorithm evaluates the water balance model 2, 000 times
114 sequentially, which may be computationally prohibitive for distributed hydrologic models with
115 longer run times. These studies break important new ground, but focus on calibrating (1) average
116 response of process over the watershed using a lumped hydrological model; (2) limited number of
117 model parameters; (3) low-to-moderate flow threshold; and (4) relatively small basins. However,
118 the computational requirement can be drastically larger for fully distributed hydrological modeling
119 over the large basin and with a large number of sensitive parameters.

120 Here we expand on previous studies and demonstrate an implementation of a Bayesian model
121 calibration framework by: (1) considering a computationally expensive distributed hydrologic
122 model; (2) taking advantage of the massive parallelization afforded by modern high-performance
123 computing systems; (3) focusing on a large number of extreme streamflow events; (4)
124 characterizing model parametric uncertainty, and (5) assessing the impacts of uncertainty
125 characterization on projected flood-hazards and -risks.

126

127 **2. Bayesian Model Calibration**

128 Various algorithms exist for characterizing hydrologic model parametric uncertainty,
129 including the multicriteria approach (Gupta et al., 1998), Generalized likelihood Uncertainty
130 Estimation (GLUE) (Beven and Binley, 1992), Shuffled Complex Evolution Metropolis algorithm
131 (SCEM-UA) (Duan et al., 1992; Sorooshian et al., 1993), Shuffled Complex Evolution Metropolis

132 (SCEM-UA) algorithm (Vrugt et al., 2003), and Differential Evolution Adaptive Metropolis
133 (DREAM) (Vrugt 2008; Laloy and Vrugt 2012; Vrugt et al., 2009), among others.

134 Bayesian computer model calibration (Bayarri et al., 2007a; Higdon et al., 2004; Kennedy &
135 O’Hagan, 2001; Sacks et al., 1989) typically addresses several (potentially overlapping)
136 objectives: (1) estimate the input parameters (in other words: what is the best parameter estimates);
137 (2) quantify the parametric uncertainty (in other words: what is the joint probability density
138 function of the parameters); and (3) infer the parameters of the observational error model and
139 discrepancy terms. These parameter estimates are impacted by factors such as model-observation
140 discrepancy (Bayarri et al., 2007b; Brynjarsdóttir & O’Hagan, 2014; Kennedy & O’Hagan, 2001)
141 and measurement errors. The Bayesian model calibration framework (see the discussion in
142 Kennedy and O’Hagan, 2001) facilitates both parameter estimation and uncertainty quantification
143 while also accounting for external sources of uncertainty (e.g., discrepancy and measurement
144 errors). For each model parameter, we specify prior distributions based on expert knowledge and
145 then update the priors by comparing the model runs to the observed data. The update proceeds by
146 placing more weight on the parameter sets whose corresponding model runs align better with the
147 observations. The resulting posterior (updated) distribution naturally provides both point and
148 interval estimates of the model parameters in light of the newly acquired data. Let $\boldsymbol{\theta}$ be the vector
149 of the model parameters, σ^2 the variance of the (assumed) independent and identically distributed
150 observational error, and $\boldsymbol{\delta}$ the discrepancy term. The posterior distribution $\tilde{\pi}(\boldsymbol{\theta}, \sigma^2, \boldsymbol{\delta} | \mathbf{Z})$ is defined
151 as:

$$\tilde{\pi}(\boldsymbol{\theta}, \sigma^2, \boldsymbol{\delta} | \mathbf{Z}) \propto L(\boldsymbol{\theta}, \sigma^2, \boldsymbol{\delta} | \mathbf{Z}) \times \pi(\boldsymbol{\theta}) \times \pi(\sigma^2) \times \pi(\boldsymbol{\delta}),$$

152 where $\tilde{\pi}(\boldsymbol{\theta}, \sigma^2, \boldsymbol{\delta} | \mathbf{Z})$ and $\pi(\cdot)$ denotes the probability density function of the posterior and prior
153 distributions, respectively. $L(\boldsymbol{\theta}, \sigma^2, \boldsymbol{\delta} | \mathbf{Z})$ is the likelihood function based upon the hydrological
154 model output, discrepancy term, and the observational error model (see Appendix).

155 For complex deterministic models, the posterior distribution may not be available in closed
156 form (Higdon, 2003; Oakley, 2009). In this case, a common approach is to approximate the
157 posterior via sampling approaches such as Markov chain Monte Carlo (MCMC) or Sequential
158 Monte Carlo. The choice of sampling approaches is influenced by several factors including: (1)
159 the computational time requirements for a single model evaluation; (2) the number of model
160 parameters to be calibrated, (3) the degree to which the algorithm can be parallelized, (4) the
161 available computation environment, and (5) the available time for the computations. Markov chain
162

163 Monte Carlo methods with the true model can be an excellent choice for models with short single
164 model run times (Asher et al., 2015; Gramacy, 2020; Lee et al., 2020). Surrogate modeling (i.e.
165 emulation-calibration) approaches replace the hydrologic model with a faster surrogate model
166 within the calibration framework; however, constructing a high-fidelity surrogate model may be
167 computationally prohibitive for high-dimensional input spaces (X. Liu and Guillas 2017; Gramacy
168 2020). Sequential Monte Carlo (SMC) (Lee et al. 2020; Kalyanaraman et al. 2016; Papaioannou,
169 Papadimitriou, and Straub 2016; Kantas, Beskos, and Jasra 2014; Morzfeld et al. 2018) methods
170 can be a practical alternative for calibrating hydrological models with a larger number of input
171 parameters.

172

173 **2.1. The Fast Model Calibrations (FaMoS) approach**

174 We use a sequential Monte Carlo particle-based approach that relies on massive
175 parallelization afforded by a high-performance computing system to efficiently calibrate a
176 distributed hydrologic model in a relatively large watershed with a number of extreme events.

177 **Fast Model Calibrations (FaMoS)** approach (Lee et al., 2020) provides an approximation of
178 the posterior distribution by (i) generating an adaptive posterior incorporation schedule to preserve
179 particle diversity; (ii) requiring very few Metropolis-Hastings updates in the mutation stages;
180 and (iii) lending itself to parallel operations distributed across thousands of processors. We
181 provide technical details about FaMoS in the Appendix.

182 FaMoS approximates the posterior distribution of the model parameters using a series of
183 sampling, reweighting, and re-sampling steps. The basic premise of sampling-importance
184 resampling (Gordon et al., 1993) is to draw independent samples from the model parameters' prior
185 distribution and retain the parameter sets whose corresponding outputs closely resemble the actual
186 observations. Each parameter set is then assigned weights, which are proportional to the likelihood
187 function $L(\boldsymbol{\theta}|\mathbf{Z})$. The parameter sets whose model outputs fit the observed data well are given
188 larger weights and those that do not are assigned smaller weights. The (importance) weights
189 $w(\boldsymbol{\theta})$ are defined as:

$$190 \quad w(\boldsymbol{\theta}) = \frac{f(\boldsymbol{\theta})}{q(\boldsymbol{\theta})} = \frac{\tilde{\pi}(\boldsymbol{\theta}|\mathbf{Z})}{\pi(\boldsymbol{\theta})}, \quad (1)$$

191 where $f(\boldsymbol{\theta})$ is the target function and $q(\boldsymbol{\theta})$ is the importance function. In this context, we specify
192 the target function as the posterior distribution of the model parameters $\tilde{\pi}(\boldsymbol{\theta}|\mathbf{Z})$ and importance

193 function as the prior distribution of the parameters $\pi(\boldsymbol{\theta})$. We approximate $\tilde{\pi}(\boldsymbol{\theta}|\mathbf{Z})$ using the
 194 weighted empirical distribution $\hat{\pi}(\boldsymbol{\theta}|\mathbf{Z})$ defined as:

$$195 \quad \tilde{\pi}(\boldsymbol{\theta}|\mathbf{Z}) \approx \hat{\pi}(\boldsymbol{\theta}|\mathbf{Z}) = \sum_{i=1}^N w(\boldsymbol{\theta}^{(i)})\delta(\boldsymbol{\theta}^{(i)}), \quad (2)$$

196 where $w(\boldsymbol{\theta}^{(i)})$ is the importance weight and $\delta(\boldsymbol{\theta}^{(i)})$ is a Dirac measure at $\boldsymbol{\theta}^{(i)}$ for the i -th sample.

197 In the fast particle-based approach (Lee et al. 2020), we draw an initial ensemble of model
 198 parameters (particles) from the prior distribution (i.e., importance function) and approximate the
 199 posterior distribution (target function) using the initial ensemble. When there is very little overlap
 200 in the high-probability regions of the prior and posterior distribution, the initial ensemble may not
 201 adequately approximate the posterior distribution due to: (1) weight degeneracy, where the vast
 202 majority of particles have near-zero weights; and (2) sample impoverishment, where we
 203 “resample” the existing particles based on the weights, and we are left with multiple copies of a
 204 few unique particles. When there is very little overlap in the high-probability regions of the prior
 205 and posterior distribution, the initial ensemble may not adequately approximate the posterior
 206 distribution due to: (1) weight degeneracy, where the vast majority of particles have near-zero
 207 weights; and (2) sample impoverishment. Sample impoverishment occurs when we are left with
 208 multiple copies of a few unique particles after a “resampling” stage. In FaMoS, the resulting
 209 particles are “resampled” through multinomial sampling based on the importance weights $w(\boldsymbol{\theta}_i)$
 210 then “mutated” or “jittered” using Metropolis-Hastings updates. Please see the Appendix for
 211 additional details.

212 FaMoS (Lee et al, 2020) mitigates these issues by gradually building up to the posterior
 213 distribution, a technique from iterated batch importance sampling (Chopin, 2002) and Sequential
 214 Monte Carlo. Here, we consider a series of intermediate posterior distributions where those earlier
 215 in the series closely resemble the prior distribution and those at the latter part better resemble the
 216 full posterior distribution. In the first cycle, we use particles from the prior distribution to
 217 approximate an earlier intermediate posterior distribution. In the subsequent cycles, we use
 218 samples from an intermediate posterior distribution to approximate a later intermediate posterior
 219 distribution. We end the algorithm when the target distribution is the final posterior distribution.
 220 For cycles $t=1, \dots, T$, the t -th intermediate posterior distribution is:

$$221 \quad \tilde{\pi}_t(\boldsymbol{\theta}|\mathbf{Z}) \propto L(\mathbf{Z})^{\gamma_t} \times \pi(\boldsymbol{\theta}), \quad (3)$$

222 where γ_t denotes the incorporation factor such that $0 = \gamma_0 \leq \gamma_1 \leq \dots \leq \gamma_{T-1} \leq \gamma_T = 1$. Note that
 223 the 0-th intermediate posterior distribution ($\tilde{\pi}_0(\boldsymbol{\theta}|\mathbf{Z})$) is simply the prior distribution $\pi(\boldsymbol{\theta})$ with

224 incorporation factor $\gamma_0 = 0$. Likewise, the T-th intermediate posterior distribution $\tilde{\pi}_T(\boldsymbol{\theta} | \mathbf{Z})$ is the
 225 full posterior distribution since $\gamma_T = 1$. At each time t , the target distribution is the t -th intermediate
 226 posterior distribution $\tilde{\pi}_t(\boldsymbol{\theta} | \mathbf{Z})$, and the prior is the intermediate posterior from the previous
 227 iteration $\tilde{\pi}_{t-1}(\boldsymbol{\theta} | \mathbf{Z})$.

228 At the end of each cycle, there still may be many replicates of a few unique particles, or
 229 sample impoverishment. To increase the number of unique particles, we “jitter” or “mutate” the
 230 particles through a carefully constructed kernel function (Gilks & Berzuini, 2001; Li et al., 2014;
 231 Liu & West, 2001). To increase the number of unique particles at the end of each cycle (t), we
 232 “jitter” or “mutate” the particles through a carefully constructed kernel function (Gilks & Berzuini,
 233 2001; Li et al., 2014; Liu & West, 2001). Upon completion of the fast particle-based calibration
 234 algorithm, we are left with an ensemble of updated parameter sets (particles) which sensibly
 235 approximate the posterior distribution. Lee et. al. (2020) also provides guidelines for choosing the
 236 number of cycles, how to mutate the particles, and how to construct these intermediate posterior
 237 distributions. We approximate the posterior distribution using “mutated” samples from the final
 238 (T-th) intermediate posterior distribution:

$$239 \quad \tilde{\pi}(\boldsymbol{\theta} | \mathbf{Z}) = \tilde{\pi}_T(\boldsymbol{\theta} | \mathbf{Z}) \approx \sum_{i=1}^N w_T(\hat{\boldsymbol{\theta}}^{(i)}) \delta(\hat{\boldsymbol{\theta}}^{(i)}) \quad (4)$$

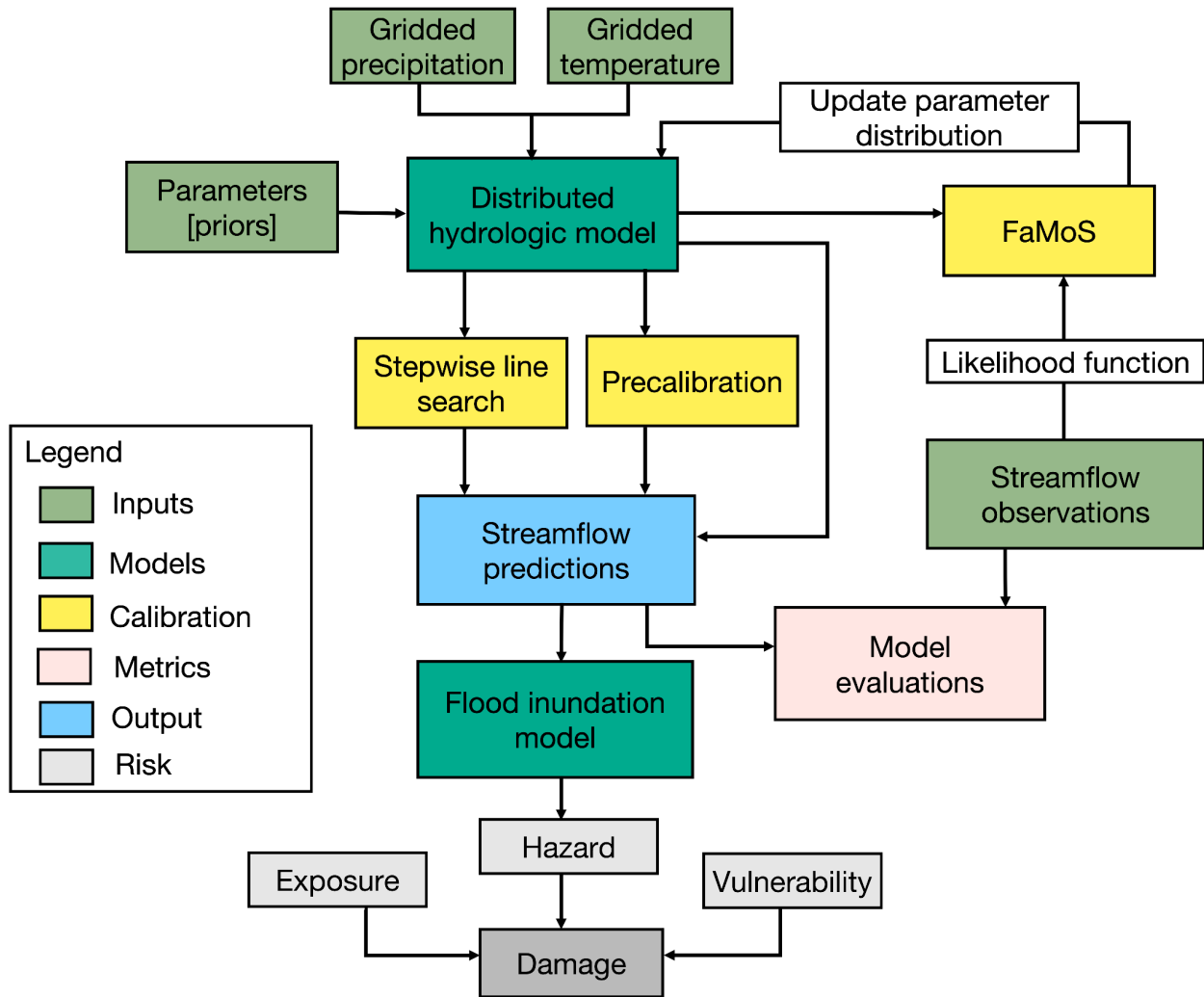
240 where $\hat{\boldsymbol{\theta}}^{(i)}$ is the i -th mutated particle, $w_T(\hat{\boldsymbol{\theta}}^{(i)})$ are the corresponding weights from the T-th cycle,
 241 and $\delta(\hat{\boldsymbol{\theta}}^{(i)})$ is a Dirac measure at $\hat{\boldsymbol{\theta}}^{(i)}$.

242

243 3. Experimental Design

244 We demonstrate the approach for a case study in the Susquehanna River basin, Pennsylvania,
 245 United States. Pennsylvania provides a relevant study area as it ranked second, tenth, and
 246 fourteenth in the United States in terms of the frequency of flash flood-related fatalities, injuries,
 247 and casualties in 1959-2005 (Ashley & Ashley, 2008). This region has experienced several
 248 devastating flooding events over the recent decades, including floods associated with the remnants
 249 of Hurricane Ivan (September 2004), late winter–early spring extratropical systems (April 2005),
 250 warm-season convective systems (June 2006), and tropical storm Lee (September 2011) (Gitro et
 251 al., 2014; Grumm, 2011). In Pennsylvania, the Federal Emergency Management Agency (FEMA)
 252 paid \$953 million in property damages to National Flood Insurance Program participants between
 253 1975 and 2019 (FEMA, 2019).

254



255

256

257 **Figure 1:** Diagrammatic representation of distributed hydrological model calibration framework.

258 The framework also demonstrates flood hazards and risk components.

259

260 We use the National Oceanic and Atmospheric Administration's (NOAA) Hydrology

261 Laboratory-Research Distributed Hydrologic Model (HL-RDHM) (Koren et al., 2004). Distributed

262 hydrologic modeling accounts for the spatial variability of model inputs, parameters and states to

263 analyze rainfall-runoff processes at desired locations within a river basin. Distributed modelling

264 involves processing and storing large amounts of data required to solve numerous and complex

265 physics-based equations at each grid cell. We run HL-RDHM in a fully distributed mode at a

266 spatial resolution of 2 km. The 2×2 km² resolution mainly allows for a more realistic

267 representation of the stream network. Within HL-RDHM, we use the Sacramento Soil Moisture

268 Accounting model with Heat Transfer (SAC-HT) (Koren et al., 2004) to represent hillslope
269 rainfall-runoff processes, and the SNOW-17 module (Anderson et al., 2006) to represent snow
270 accumulation and melt. SAC-HT is a physics-based, conceptual model where the basin system is
271 divided into regularly spaced, square grid cells to account for spatial heterogeneity and variability.
272 Each grid cell, in turn, is composed of storage components that store and transmit water. The cells
273 are ultimately connected to each other through the stream network system, that is, each cell acts as
274 a hillslope capable of generating surface and subsurface runoff that discharges directly into the
275 streams. The hillslope runoff, generated at each grid cell by the SAC-HT and SNOW-17, is routed
276 to the stream network using a nonlinear kinematic wave algorithm (Koren et al., 2004). Further
277 information about the HL-RDHM model can be found for example in Koren et al. (2004), Reed et
278 al. (2004), and Anderson et al. (2006). The HL-RDHM distributed hydrological model takes
279 approximately 15 minutes per run on a single 2.3-GHz Intel Xeon E5-2697V4 (Broadwell)
280 processor on the Cheyenne cluster (Computational and Information Systems Laboratory, 2017).

281 We use three main datasets: multisensor precipitation estimates, gridded near-surface air
282 temperature, and streamflow. We use NOAA's multisensor precipitation estimates and gridded
283 near-surface air temperature products to run the hydrological model for parameter calibration
284 purposes and to initialize the model. Multisensor precipitation estimates represent a continuous
285 time series of hourly, gridded precipitation observations at 4×4 km² cells, which are produced by
286 combining multiple radar estimates and *in situ* rain-gauge measurements (Prat & Nelson, 2015;
287 Rafieeiniasab et al., 2015). The gridded near-surface air temperature data are derived by combining
288 multiple temperature observation networks, including the meteorological terminal aviation routine
289 weather report (METAR), USGS stations, and National Weather Service Cooperative Observer
290 Program (Siddique & Mejia, 2017). We use streamflow observations from the United States
291 Geological Survey gage 01554000 located at Susquehanna River at Sunbury, Pennsylvania. The
292 selected gage station represents the drainage area of 47,396 km².

293 We calibrate the model for the period of 2004-2008 and use 2009-2012 observations to
294 evaluate the calibration performance. We use the year 2003 to spin up the model. As part of the
295 calibration process, we select 12 out of the 17 model parameters associated with each model grid
296 cell (Table S1). To improve calibration efficiency, basin-scale parameter multipliers, rather than
297 the parameters in each grid, were calibrated and applied to the a-priori parameter grids (NWS,
298 2011). We only consider the model parameters that have a strong influence on the model output

299 (see Figure S1). Exploring a higher-dimensional parameter space demands additional processors
300 (particles) (Bain & Crisan, 2008; Jeremiah et al., 2011; Kantas et al., 2014) to sensibly calibrate
301 the hydrological model. Selecting only the strongly influential model parameters can help reduce
302 the computational costs considerably. This is, of course, an approximation and points to future
303 research needs. The sensitive parameters are associated with different hydrodynamic processes
304 related to baseflow, percolation, evaporation, snowfall, storm runoff, and channel routing (Table
305 S1). These parameters are also suggested by several other studies (Gomez et al., 2019; Sharma et
306 al., 2021; Siddique & Mejia, 2017; Zarzar et al., 2018) as the most sensitive parameters in the
307 Susquehanna river basin.

308 We compare Bayesian calibration with relatively simple and low-cost model calibration
309 approaches: i) stepwise line search (Kuzmin et al., 2008) and ii) precalibration (Edwards et al.,
310 2011). Stepwise line search typically adjusts a subset of model parameters to minimize an objective
311 function (e.g., root mean square error) and returns a single estimate of the model parameters (for
312 details of the implementation please see Text S2) (Bowman et al., 2017; Carlberg et al., 2020;
313 Fares et al., 2014; Mejia & Reed, 2011; Siddique & Mejia, 2017). Precalibration applies a
314 screening criterion to a large ensemble of hydrologic model runs and rules out any implausible
315 model runs that deviate substantially from the observations (refer Text S3 for the details) (Craig
316 et al., 1997; Edwards et al., 2011; Holden et al., 2010; Tarawneh et al., 2016). These simple
317 approaches of carrying out limited calibration are used by many academic studies (Rafieenasab
318 et al., 2015; Siddique and Mejia, 2017; Fares et al., 2014; Kim et a., 2021) as well as commonly
319 practiced in real-word applications (Salas et al., 2018). They are used in part because they are
320 simple and fast (Knutti et al., 2002; Reed et al., 2022).

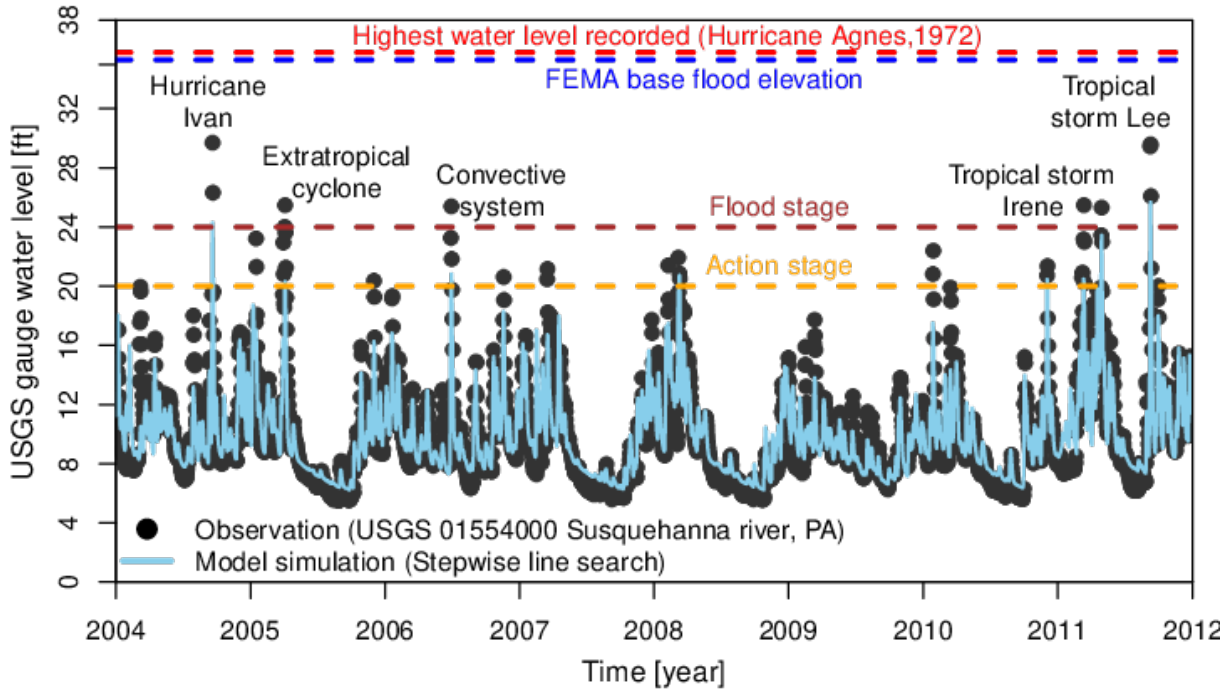
321 We evaluate the calibrated model performance using several decision-relevant metrics. We
322 use traditional deterministic metrics such as the Kling-Gupta Efficiency (KGE) (Mizukami et al.,
323 2019), which provides a direct assessment of streamflow time series (e.g., shape, timing, water
324 balance and variability) using the ensemble mean estimate. We also evaluate the probabilistic
325 prediction skill using the Brier Skill Score (BSS) (Murphy, 1973) and the Continuous Ranked
326 Probability Skill Score (CRPSS) (Murphy, 1970). The Brier score is essentially the mean squared
327 error of the probability predictions, considering that the observation is one if the event occurs, and
328 that the observation is zero if the event does not occur. The Continuous Ranked Probability Score
329 measures the integral square difference between the cumulative distribution functions of the

330 observation and predictions, averaged over all pairs of predictions and observations. The selection
331 of these decision-relevant metrics is motivated by the balance between model output goodness-of-
332 fit, calibration approaches, and data availability. The description of evaluation metrics is provided
333 in Text S4 in the supporting information. Model calibration and evaluation is focused on high
334 flows by choosing the river flow that exceeds NOAA's Action Stage (McEnery et al., 2005).
335 Action Stage refers to the stage which, when reached by a rising river, represents the level where
336 the National Weather Service or a partner/user needs to take some mitigation action in preparation
337 for possible significant hydrologic activity.

338 We assess the impact of model calibration on flood damage estimates. Flood damage
339 represents interactions among hazard, exposure and vulnerability (Tellman et al., 2021; Wing et
340 al., 2018). Hazard in this case refers to the magnitude of the flood event. Exposure characterizes
341 property value in the floodplain. Vulnerability characterizes how sensitive the impacts are for a
342 given hazard and exposure. We consider 2,000 hypothetical houses to quantify the damage from
343 flood hazards (Figure S4; TextS6). We assess damage for a certain depth of water in a house by
344 using a relatively simple Bathtub-based flood inundation model (Didier et al., 2019; Fereshtehpour
345 & Karamouz, 2018; Neumann & Ahrendt, 2013; Yunus et al., 2016) and a vulnerability model
346 (Scawthorn et al., 2006). The Bathtub model relies on a digital elevation model to provide flood
347 depth in a house for a particular corresponding water level in the river (refer TextS5 and TextS6
348 for the details). We use a common vulnerability model (depth-damage function) provided by the
349 Federal Emergency Management Agency (FEMA) (Scawthorn et al., 2006).

350 **4. Results and Discussion**

351 We first generate streamflow simulations using the "best" parameter estimates obtained via
352 the stepwise line search (Figure 2). In the considered example, stepwise line search substantially
353 underestimates the high streamflow (Figure 2). Stepwise line is designed to sample high-
354 probability outcomes and excludes comprehensive sampling of the parametric distribution
355 (Kuzmin et al., 2008; Sharma et al., 2019).



356

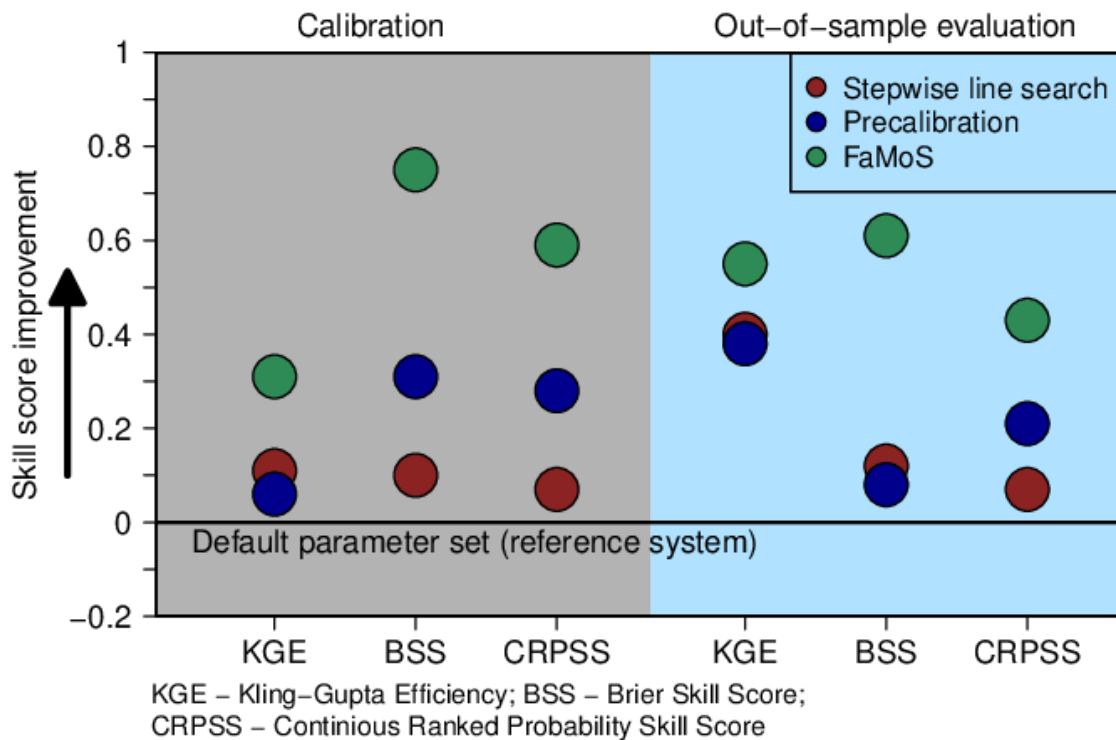
357 **Figure 2:** Historical time series of water level observation and model simulations obtained using
 358 best parameter estimates (stepwise line search). We obtain the observation from the United States
 359 Geological Survey (USGS) gauge records for ID 01554000 located upstream of Selinsgrove,
 360 Pennsylvania, USA. The most destructive floods in the Susquehanna river basin that occurred in
 361 recent years, each associated with different flood-generating mechanisms, includes Hurricane Ivan
 362 (September 2004), late winter–early spring extratropical systems (April 2005), warm-season
 363 convective systems (June 2006), and tropical storm Lee (September 2011).

364

365 We account for parametric uncertainty using precalibration and FaMoS (Figure S1).
 366 Characterizing parametric uncertainty requires knowledge of model behavior throughout the (often
 367 high-dimensional) parameter space. Precalibration provides a relatively simple method to explore
 368 the high-dimensional parameter space. Precalibration is a low-cost way of ruling out implausible
 369 model runs. We begin with an initial ensemble of 5,000 model runs with input parameters settings
 370 selected from a 12-dimensional Latin hypercube design (Helton & Davis, 2003). We select an
 371 ensemble of 165 runs that fall within the +/- 75% window surrounding each observation. Note that
 372 specifying bounds for precalibration is a subjective choice (Craig et al., 1997; Edwards et al., 2011;
 373 Holden et al., 2010; Tarawneh et al., 2016). This choice impacts the “surviving” parameter
 374 samples. For instance, imposing tight bounds on the observed streamflow could lead to high-

375 resolution sampling of the plausible parameter space and wider bounds may include more
 376 implausible runs into the final ensemble. We choose the considered acceptable range to sample
 377 into the upper tails of projected flood hazards, which are often associated with high-cost events.

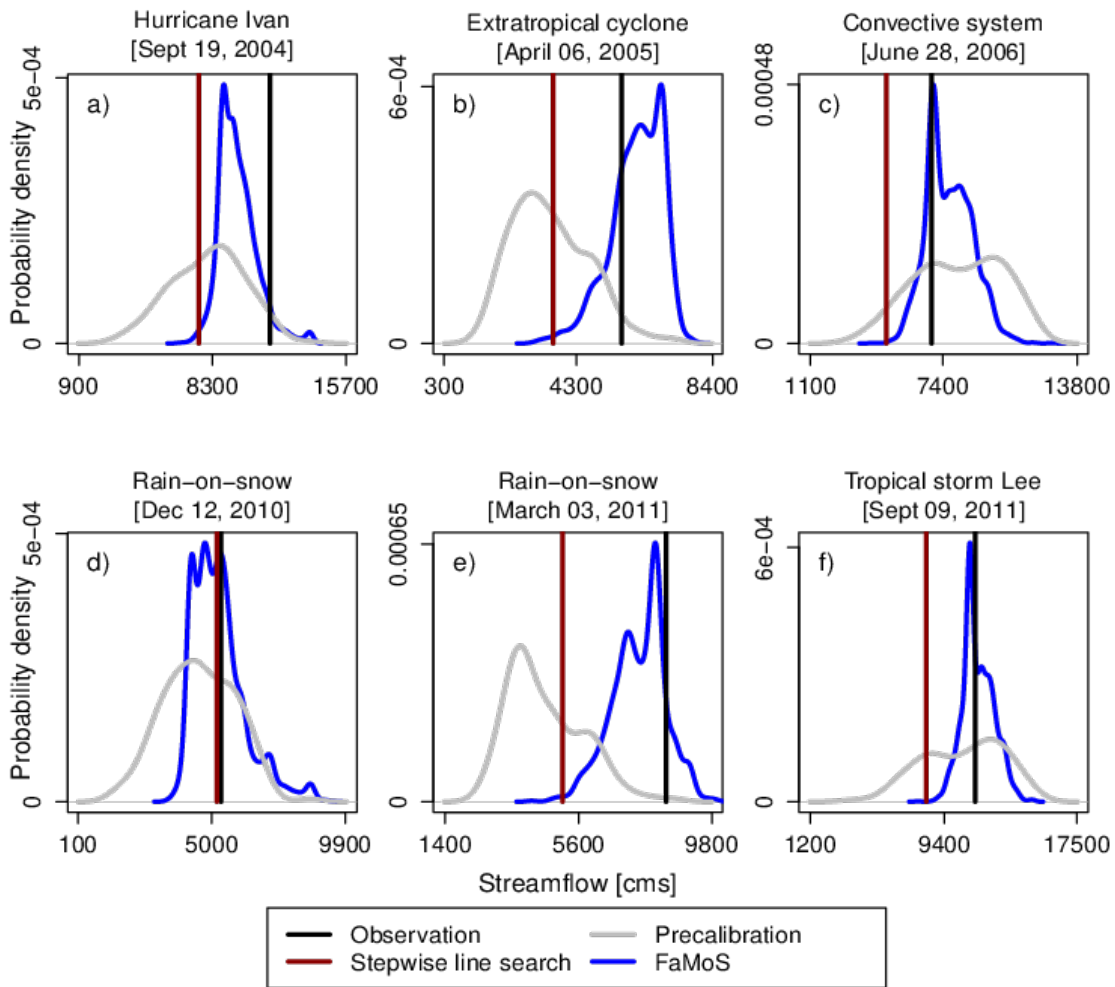
378 FaMoS adopts a more complex (but also more powerful) calibration approach compared to
 379 precalibration. We incorporate domain-area expertise (prior distribution) of the unknown
 380 parameters and also account for additional sources of uncertainty such as model-observation
 381 discrepancies and observational error (see the Appendix for the details). As a result, we obtain a
 382 distribution of viable parameter values (posterior distribution) along with interval estimates, as
 383 opposed to a single best fit estimate (Figure S1). Unlike precalibration, FaMoS does not fix an
 384 arbitrary screening criterion, but rather uses a flexible statistical model to assess model-fit.
 385 Moreover, FaMoS sequentially explores the entire parameter space and systematically attempts to
 386 move to a “target” region that contains the most plausible sets of model parameters. In contrast,
 387 precalibration attempts to locate this “target” region using a single initial ensemble of model runs.



388
 389 **Figure 3:** Performance metrics for hydrological model calibration and out-of-sample prediction.
 390 We compute Kling-Gupta Efficiency (KGE), and Brier skill score (BSS), and mean Continuous
 391 ranked probability skill score (CRPSS). All the metrics are computed with reference to the default
 392 parameter set available from several previous studies (Anderson et al. 2006, Reed et al. 2004). Any

393 positive values of the skill score, from 0 to 1, indicate that the calibration approach performs better
394 than the reference system. Thus, a skill score of zero indicates no skill, and a skill of one indicates
395 perfect skill. We plot the average value to compute KGE. CRPSS measures the integrated squared
396 difference between the cumulative distribution function (cdf) of a model prediction, and the
397 corresponding cdf of the observations. The CRPSS is averaged across n pairs of model predictions
398 and observations, which leads to the mean CRPSS. BSS measures the averaged squared error of a
399 probability prediction.

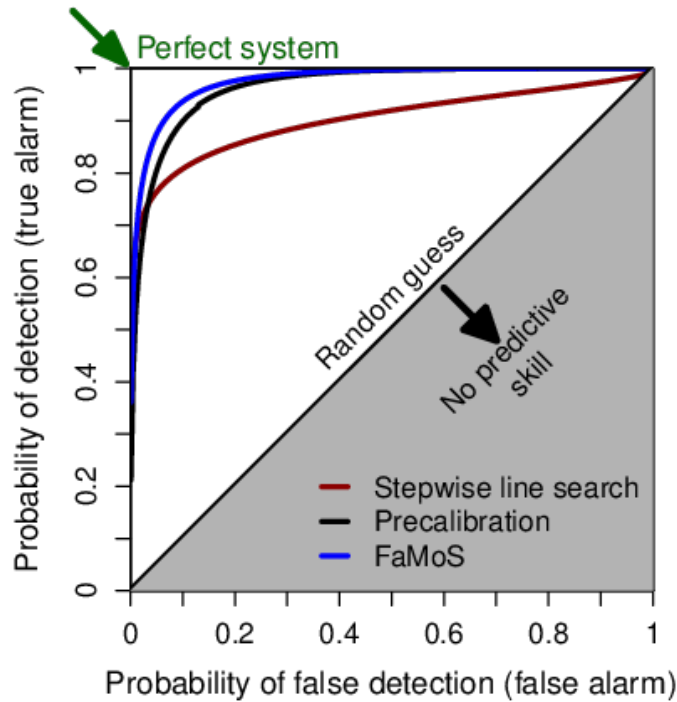
400
401 Accounting for parametric uncertainty improves model performance metrics for the
402 calibration data and out-of-sample predictions (Figure 3). We compute the skill score (KGE, BSS,
403 and CRPSS) with reference to raw (uncalibrated) model runs using default parameter estimates
404 obtained from several previous studies (Anderson et al., 2006; Reed et al., 2007). In terms of the
405 performance metrics, model predictions remain skillful for all the calibration approaches (Figure
406 3). Precalibration outperforms the stepwise line search (best estimate predictions). Stepwise line
407 search and precalibration are not designed to find the global maximum, which can lead to lower
408 skill score as compared to FaMoS. FaMoS demonstrate a higher skill score than both the stepwise
409 line search and precalibration for both calibration and out-of-sample evaluations.



410
 411 **Figure 4:** (a) - (c) Calibration and (d) - (f) and out-of-sample prediction for different flood events.
 412

413 Accounting for parametric uncertainty improves flood hazard estimates (Figure 4). The
 414 resulting predictive distribution of flood events demonstrates the impacts of model calibration. The
 415 stepwise line search underestimates the flood peaks by as much as 35% (Figure 4b) during
 416 calibration and 40% during out-of-sample prediction (Figure 4e). Precalibration captures the
 417 specific flood events, but exhibits very high prediction uncertainty as evidenced by the wider
 418 prediction intervals. Overall, FaMoS improves flood peak estimates and provides narrower
 419 prediction intervals. Consider, as an example, the case of Tropical Storm Lee with streamflow
 420 observation of 11, 292 m³/sec. Precalibration provides a flood peak prediction of 10, 539 m³/sec
 421 and prediction intervals (5%-95% credible interval) range from 6, 359 m³/sec to 14, 222 m³/sec

422 (width = 7, 863 m³/sec). FaMoS has a corresponding flood peak prediction of 11, 467 m³/sec with
423 a credible interval ranging from 9, 925 m³/sec to 13, 121 m³/sec (width = 3, 196 m³/sec).



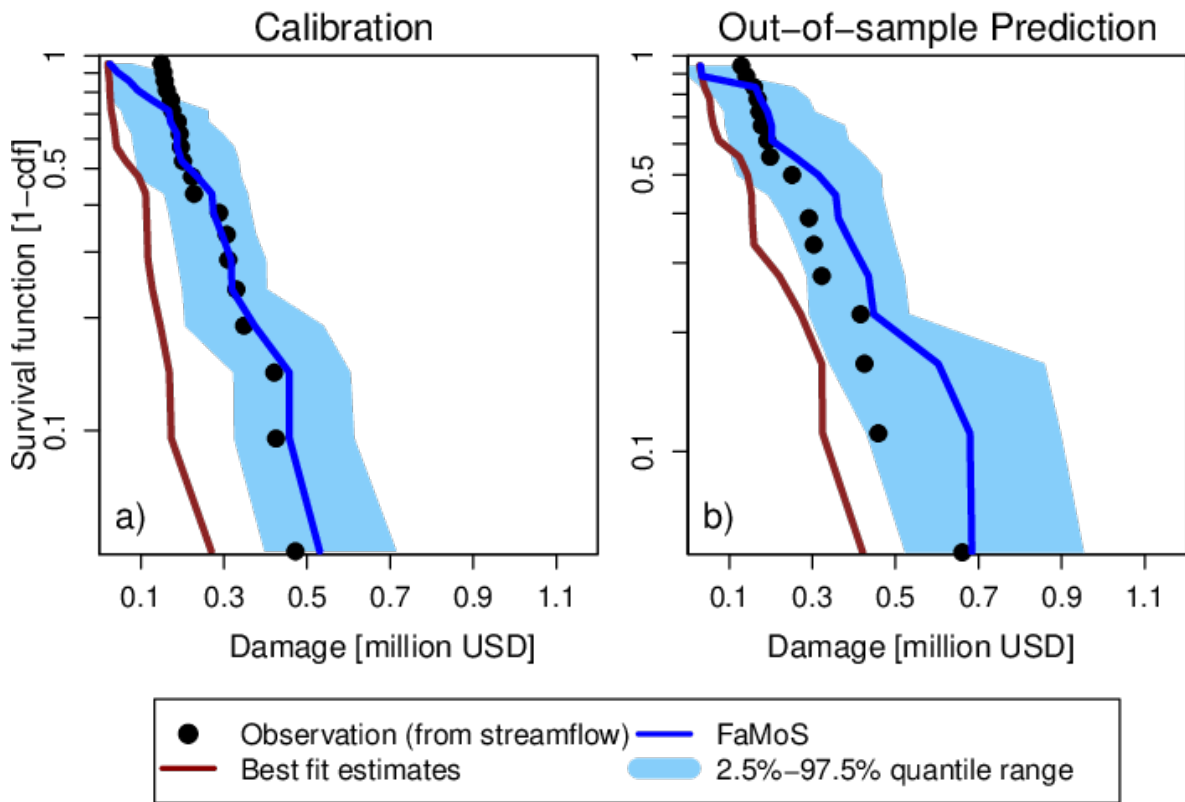
424
425

426 **Figure 5:** Relative operating characteristics (ROC) curve for different calibration approaches.
427 ROC curve plots the probability of detection against the probability of false detection for a range
428 of forecast probability levels. A larger area under the ROC curve represents a more skillful
429 prediction, with more ability to discriminate between flood thresholds. The area under the ROC
430 curve can range between 0 and 1, where a score of 1 implies perfect discrimination and a score of
431 0.5 or less implies predictive discrimination that is no better than a random guess. We also compute
432 the ROC score. The ROC score measures the average gain over climatology for all probability
433 levels. The ROC score for stepwise line search, precalibration and FAMOS is 0.55, 0.85 and 0.96
434 respectively.

435

436 We assess each calibration approach's classification ability or how well each method
437 discriminates between occurrences (water level crossing the action stage) versus non-occurrences
438 (regular water level) of an event (Figure 5). Managing flood risks can require decision makers to
439 choose between two options (e.g., to evacuate or not or to elevate a house or not) based on a

440 prediction of an event (e.g., water rising to a certain level) with one decision preferred if the event
 441 doesn't occur, and the other if it does. A perfect prediction system for a binary outcome correctly
 442 predicts the occurrence of an event (unity probability of detection) and never issues incorrect
 443 predictions when it does not occur (zero probability of false detection). How well a prediction
 444 system approaches this ideal case can be quantified by the relative operating characteristics (ROC)
 445 curve (see Text S4) (Mason & Graham, 2002). Technically, the ROC curve assesses the quality of
 446 probability predictions by relating the probability of detection (true alarm) to the corresponding
 447 probability of false detection (false-alarm rate), as a decision threshold is varied across the full
 448 range of a continuous prediction quantity (Figure 5). We fix the threshold corresponding to the
 449 river flow that exceeds NOAA's Action Stage. Streamflow predictions obtained using FaMoS
 450 parameter distribution exhibit better discriminatory ability (higher ROC score) than the stepwise
 451 line search and precalibration. Stepwise line search shows a relatively poor ability to discriminate
 452 between different events. This poor ability to discriminate between the events can lead to poor
 453 decisions and outcomes.



454
 455 **Figure 6:** Survival function (one minus the cumulative frequency) for damage estimates using
 456 streamflow obtained using the best parameter set (stepwise line search) and parameter distribution

457 (FaMoS). We show damage estimates for a) calibration and b) out-of-sample prediction. cdf=
458 cumulative distribution function.

459

460 Neglecting parametric uncertainty also underestimates potential flood damage (Figure 6). We
461 find that the stepwise line search tends to underestimate the flood damage. The underestimation
462 bias increases as flood magnitude increases. Accounting for parametric uncertainty improves the
463 damage estimates for the calibration data and out-of-sample predictions. The damage credible
464 interval obtained using FaMoS parameter distribution generally captures the observed damage for
465 different flood events. As expected, at the upper tails of the damage, the predictive uncertainty
466 tends to be higher for the out-of-sample prediction as compared to the calibration.

467

468 **5. Caveats**

469 We use a relatively simple model and small region with hypothetical exposure to demonstrate
470 our points. This parsimony helps with transparency, but it comes with several caveats. For
471 example, our analysis focuses on calibrating high flows by choosing the river flow that exceeds
472 NOAA's Action Stage. Temporal independence, conditioned on the model outputs, is a key
473 assumption within the calibration framework. We calibrate multiple disjoint (or unconnected)
474 instances of extreme streamflow events. We compute skill score to assess the performance of
475 different calibration approaches. However, implementing the Ljung-Box test and other diagnostic
476 tools for autocorrelation (Smith et al., 2015) would require calibrating a continuous streamflow
477 time series. Future work might consider calibrating a continuous time series of streamflow,
478 including low flows and moderate flows. Due to a large number of low and moderate flow
479 observations, dimension-reduction techniques like principal components (Chang et al., 2014;
480 Higdon et al., 2008) or eigenfunctions (Mak et al., 2018) may be appropriate to summarize the
481 large datasets. This study samples shallow uncertainty about hydrologic model parameters as a
482 case-study. There are, of course, other deep uncertainties (Lempert, 2002) affecting flood hazards
483 and risks that could be taken into account in future work (Mendoza et al., 2015, Bates et al., 2021,
484 Reed et al., 2022). These include model structural uncertainty, different spatial resolutions, land
485 surface characteristics, or projections of the socio-economic systems (Gupta et al., 2012; Kavetski
486 et al., 2006; Zarekarizi et al., 2020). Characterizing the individual uncertainty sources and their
487 propagation is crucial to improve the reliability of flood hazard and risk projections. Increasing the

488 spatio-temporal resolutions may drastically raise the hydrologic model’s complexity as well as the
489 associated single model run times. To reduce the number of sequential hydrologic model
490 evaluations, we can embed parallel Markov Chain Monte Carlo approaches such as Multiple-Try
491 Metropolis (Liu et al., 2000) or “emcee” samplers (Goodman & Weare, 2010) or genetic
492 algorithms (Park et al., 2009) into FaMoS calibration framework. We note that our damage
493 estimates are based on a simple Bathtub-based flood inundation model. Future work could use
494 process-informed models to characterize the impacts of hydrodynamic processes in damage
495 estimates (Brunner, 1995; Coulthard et al., 2013; Judi et al., 2018). In addition, future work could
496 sample the uncertainty surrounding the flood vulnerability of the building (Wing et al., 2020).

497 Although the objective of this study is not to compare different complex calibration
498 approaches, FaMoS can add to emerging research into uncertainty quantification of a distributed
499 hydrologic model. We demonstrate the ability of FaMoS to calibrate a large number of extreme
500 flood events and consider a relatively larger river basin than in the several previous studies (Vrugt
501 et al., 2008; Vrugt et al., 2009; Laloy and Vrugt, 2012). Computationally, the problem becomes
502 very different to run and calibrate a spatially distributed model over a large river basin. Future
503 study could compare FaMoS with other complex and state-of-the art Bayesian calibration
504 approaches (e.g., Vrugt et al., 2008).

505

506 **6. Conclusions**

507 We use a Bayesian data-model fusion framework to calibrate a distributed hydrologic
508 model and to demonstrate practical implications of neglecting key uncertainties on hazard- and
509 risk-estimates. We compare the results of the Bayesian approach to two simpler methods: stepwise
510 line search and precalibration. We show that these simpler methods can considerably
511 underestimate flood hazards and risks. Precalibration improves flood hazards estimates over the
512 best fit estimates, but provides a wider predictive interval (i.e., highly uncertain estimates) than
513 the Bayesian approach. The predictive skill of the Bayesian approach dominates the stepwise line
514 search and precalibration approaches. We show how neglecting model parametric uncertainty can
515 substantially underestimate flood hazards and risk estimates and demonstrate how applying state-
516 of-the-art statistical methods can help to refine flood-risk projections.

517 **Acknowledgments**

518 This study was co-supported by the US Department of Energy, Office of Science through the
519 Program on Coupled Human and Earth Systems (PCHES) under DOE Cooperative Agreement
520 No. DE-SC0016162 and DE-SC0022141 as well as the Penn State Center for Climate Risk
521 Management. We thank Rob Nicholas, Skip Wishbone, Dave Judi, and the PSIRC team for inputs.
522 All errors and opinions (unless cited) are those of the authors and not of the funding entities.

524 **Disclaimer and License**

525 The results, data, software tools, and other resources related to this work will be available
526 under the GNU general public open-source license, as-is, without warranty of any kind, expressed
527 or implied. In no event shall the authors or copyright holders be liable for any claim, damages, or
528 other liability in connection with the use of these resources. This is academic research and not
529 designed to be used to guide a specific decision.

531 **Author contributions**

532 All authors contributed to the study design. S.S. led the hydrologic analysis. B.L. and M.H.
533 constructed the particle-based calibration model. I.H.S led the flood damage analysis. I.H.S.
534 performed a code review. S.S., B.L, and K.K wrote the initial draft of the manuscript. All authors
535 revised and edited the manuscript. Correspondence and requests for materials should be addressed
536 to the corresponding author.

538 **Data and Code Availability**

539 The code used for this analysis and the data required to plot the results is available through a
540 publicly accessible GitHub repository and under the GNU open-access license upon acceptance to
541 a peer-reviewed journal. Reviewers can access these resources from
542 <https://github.com/bene55/FamosHydroModel>. All data and code currently available at GitHub
543 will be published via Zenodo upon article acceptance.

544 **Competing interests**

545 The authors are not aware of any competing financial or nonfinancial interests.

Appendix A: Fast Model Calibrations (FaMoS) Details

1 Bayesian Calibration Framework

Suppose we have an observed time series $\mathbf{Z} = (Z(r_1), \dots, Z(r_n))'$ times $r_i \in \mathcal{R}$ where \mathcal{R} is the temporal domain of the process. We also have a deterministic computer model that generates a temporal process, or time series, at times $r_i \in \mathcal{R}$. Let $Y(r, \boldsymbol{\theta})$ be the computer model output at the time $r \in \mathcal{R}$ and the parameter (input) setting $\boldsymbol{\theta} \in \Theta \subseteq \mathbb{R}^d$. Θ is the parameter space of the computer model with integer d being the number of input parameters. In this study, we use a discontinuous temporal domain at R distinct time points $\nabla = (r_1, \dots, r_R)'$. The vector $\mathbf{Y}(\boldsymbol{\theta}_i) = (Y(r_1, \boldsymbol{\theta}_i), \dots, Y(r_R, \boldsymbol{\theta}_i))'$ is the computer model output corresponding to parameter setting $\boldsymbol{\theta}_i$. For input parameter setting $\boldsymbol{\theta}$, we model the observations \mathbf{Z} as:

$$\mathbf{Z} = \mathbf{Y}(\boldsymbol{\theta}) + \boldsymbol{\delta} + \boldsymbol{\epsilon}, \quad (\text{A1})$$

where $\boldsymbol{\epsilon} \sim N(\mathbf{0}, \sigma_\epsilon^2 \mathbf{I})$ are the independently and identically distributed observational error, and $\boldsymbol{\delta} \in \mathbb{R}^n$ is a systemic data-model discrepancy term, which can be modeled as a zero-mean Gaussian process (Bhat et al., 2010; Bayarri et al., 2007) or other flexible functional forms (Brynjarsdottir and O'Hagan, 2014).

In the Bayesian calibration framework, we obtain samples (via a Markov chain Monte Carlo (MCMC) algorithm) from the posterior distribution:

$$\tilde{\pi}(\boldsymbol{\theta}, \sigma_\epsilon^2, \boldsymbol{\delta} | \mathbf{Z}) \propto L(\boldsymbol{\theta}, \sigma_\epsilon^2, \boldsymbol{\delta} | \mathbf{Z}) \pi(\boldsymbol{\theta}) \pi(\sigma_\epsilon^2) \pi(\boldsymbol{\delta}), \quad (\text{A2})$$

where $L(\boldsymbol{\theta}, \sigma_\epsilon^2, \boldsymbol{\delta} | \mathbf{Z})$ denotes the likelihood function and $\pi(\cdot)$ represents the prior distribution for the respective parameters and discrepancy term. Note that each evaluation of $L(\boldsymbol{\theta}, \sigma_\epsilon^2, \boldsymbol{\delta} | \mathbf{Z})$ requires running the computer model using specific input parameters $\boldsymbol{\theta}$. Hence, MCMC-based calibration approaches are sensible for computer models with shorter single model run walltimes, typically under 5 seconds per model run (Lee et al., 2020). For our study, we estimate that a standard MCMC-based calibration approach would on the order of years to approximate the posterior distribution $\tilde{\pi}(\boldsymbol{\theta}, \sigma_\epsilon^2, \boldsymbol{\delta} | \mathbf{Z})$.

2 Particle-based Calibration Framework

We calibrate the HL-RDHM distributed hydrological model using the fast particle-based approach from Lee et al. (2020), which is built upon traditional Sequential Monte Carlo algorithms (Del Moral et al., 2006; Doucet et al., 2000; Liu and West, 2001), notably the Iterated Batch Importance Sampling (IBIS) (Chopin, 2002; Crisan and Doucet, 2000) method. This method approximates the posterior distribution $\tilde{\pi}(\boldsymbol{\theta}, \sigma_\epsilon^2, \boldsymbol{\delta} | \mathbf{Z})$ using an evolving ensemble of particles.

We simplify the notation for an arbitrary target distribution as $\pi(\boldsymbol{\theta})$ with random variable $\boldsymbol{\theta} \in \mathbb{R}^d$. In the hydrological model calibration framework, the target distribution $\pi(\boldsymbol{\theta})$ would be the posterior distribution $\tilde{\pi}(\boldsymbol{\theta}, \sigma_\epsilon^2, \boldsymbol{\delta} | \mathbf{Z})$ with random variables $\boldsymbol{\theta}, \sigma_\epsilon^2$, and $\boldsymbol{\delta}$ and observations \mathbf{Z} . Suppose we want to estimate $\boldsymbol{\mu} = E_\pi[g(\boldsymbol{\theta})]$. Given $q(\boldsymbol{\theta}) > 0$ whenever $g(\boldsymbol{\theta})\pi(\boldsymbol{\theta}) > 0, \forall \boldsymbol{\theta} \in \Theta$. Then $E_\pi[g(\boldsymbol{\theta})] = E_q[g(\boldsymbol{\theta})w(\boldsymbol{\theta})]$, where $w(\boldsymbol{\theta}) = \frac{\pi(\boldsymbol{\theta})}{q(\boldsymbol{\theta})}$

35 is the importance weight and $\sum_{i=1}^N w(\boldsymbol{\theta}_i) = 1$. The importance sampling estimator is
 36 $\hat{\boldsymbol{\mu}}_n = \frac{1}{n} \sum_{i=1}^N g(\boldsymbol{\theta}_i) w(\boldsymbol{\theta}_i)$ and $\hat{\boldsymbol{\mu}}_n \rightarrow \boldsymbol{\mu}$ with probability 1 as $n \rightarrow \infty$ by the strong law of
 37 large numbers. For target distributions with an unknown normalizing constant, the weights
 38 can be normalized as follows:

$$\tilde{w}(\boldsymbol{\theta}_i) = \frac{w(\boldsymbol{\theta}_i)}{\sum_{j=1}^n w(\boldsymbol{\theta}_j)} = \frac{\pi(\boldsymbol{\theta}_i)/q(\boldsymbol{\theta}_i)}{\sum_{j=1}^n w(\boldsymbol{\theta}_j)} \quad (\text{A3})$$

39 where $\sum_{i=1}^N \tilde{w}(\boldsymbol{\theta}_i) = 1$.

40 Sampling-Importance-Resampling (Gordon et al., 1993; Doucet et al., 2001) approxi-
 41 mates a target distribution $\pi(\boldsymbol{\theta})$ with an empirical distribution of the particles $\hat{\pi}(\boldsymbol{\theta})$ from an
 42 importance function $q(\boldsymbol{\theta})$ such as the prior distribution. The empirical distribution $\bar{\pi}(\boldsymbol{\theta})$ is
 43 defined as:

$$\bar{\pi}(\boldsymbol{\theta}) = \sum_{i=1}^N \tilde{w}(\boldsymbol{\theta}_i) \delta(\boldsymbol{\theta}_i) \approx \pi(\boldsymbol{\theta}), \quad (\text{A4})$$

44 where $\tilde{w}(\boldsymbol{\theta}_i)$ are the normalized importance weights, $\delta(\boldsymbol{\theta}_i)$ is a Dirac measure that places
 45 unit mass at $\boldsymbol{\theta}_i$ and $\sum_{i=1}^N \tilde{w}(\boldsymbol{\theta}_i) = 1$.

46 Poor choices of importance functions can lead to inaccurate approximations of the target
 47 distribution (Doucet et al., 2000) where the bulk of the particles $\boldsymbol{\theta}_i$'s do not reside in the
 48 high-probability regions of the target distribution $\pi(\boldsymbol{\theta})$. Weight degeneracy occurs when the
 49 vast majority of the particles have near-zero importance weights. Multinomial resampling
 50 methods can combat weight degeneracy by eliminating the particles with very small impor-
 51 tant weights and replicating those with higher weights (Gordon et al., 1993; Doucet et al.,
 52 2000). After resampling, we reset all importance weights such that $w(\boldsymbol{\theta}_i) = 1/N$ and use
 53 the unweighted empirical distribution $\ddot{\pi}(\boldsymbol{\theta})$:

$$\ddot{\pi}(\boldsymbol{\theta}) = \frac{1}{N} \sum_{i=1}^N N_i \delta(\boldsymbol{\theta}_i), \quad (\text{A5})$$

54 where N_i is the number of replicates corresponding to particle $\boldsymbol{\theta}_i$ and $\sum_{i=1}^N N_i = N$. Extreme
 55 weight degeneracy, where very few particles have any significant weight, can lead to sample
 56 impoverishment where a few unique particles $\boldsymbol{\theta}_i$'s are heavily replicated in the re-sampling
 57 step; hence, the empirical distribution $\ddot{\pi}(\boldsymbol{\theta})$ may poorly approximate the target distribution
 58 $\pi(\boldsymbol{\theta})$.

59 An alternative method mutates the replicated particles with samples from $K(\boldsymbol{\theta}_i^{(t-1)})$, the
 60 Metropolis-Hastings transition kernel (Gilks and Berzuini, 2001), whose stationary distribu-
 61 tion is also the target distribution $\pi(\boldsymbol{\theta})$. The mutation stage proceeds with K Metropolis-
 62 Hastings updates for each particle $\boldsymbol{\theta}_i$, for $i = 1, \dots, N$. Alternative mutation schemes use
 63 genetic algorithms (Zhu et al., 2018) or different families of transition kernels, $K(\cdot)$ (Pa-
 64 paioannou et al., 2016; Murray et al., 2016). We set the K -th sample drawn via MCMC as
 65 the mutated particle $\tilde{\boldsymbol{\theta}}_i$. Since $\tilde{\boldsymbol{\theta}}_i \sim \pi(\boldsymbol{\theta})$, the resulting empirical distribution $\hat{\pi}(\boldsymbol{\theta})$ approxi-
 66 mates the target distribution $\pi(\boldsymbol{\theta})$:

$$\pi(\boldsymbol{\theta}) \approx \hat{\pi}(\boldsymbol{\theta}) = \sum_{i=1}^N \tilde{\boldsymbol{\theta}}_i \delta(\tilde{\boldsymbol{\theta}}_i). \quad (\text{A6})$$

67 Unfortunately, poor importance functions can result in severe sample impoverishment,
 68 which may require very long (and costly) mutation stages to provide an accurate represen-
 69 tation of the target distribution (Li et al., 2014). Mixture approximations (Gordon et al.,
 70 1993) or kernel smoothing methods (Liu and West, 2001) can mutate or rejuvenate the
 71 replicated particles. However, these methods may not scale well to high-dimensional target
 72 distributions (Doucet et al., 2000).

73 2.1 Fast Particle-based Approach For Computer Model Calibra- 74 tion

75 In this study, we aim to approximate the posterior $\tilde{\pi}(\boldsymbol{\theta}, \boldsymbol{\delta}, \sigma_\epsilon^2 | \mathbf{Z})$ from a computationally effi-
 76 cient approach. The fast particle-based approach (Lee et al., 2020) utilizes a set of tempered,
 77 or intermediate, posterior distributions $\tilde{\pi}_t(\boldsymbol{\theta}, \boldsymbol{\delta}, \sigma_\epsilon^2 | \mathbf{Z})$ for $t = 1, \dots, T$, which will act as both
 78 the importance functions and target distributions. Intermediate posterior distributions can
 79 be generated using likelihood tempering (Chopin, 2002; Neal, 2001; Liang and Wong, 2001)
 80 where the t th intermediate posterior distribution is defined as:

$$\tilde{\pi}_t(\boldsymbol{\theta}, \boldsymbol{\delta}, \sigma_\epsilon^2 | \mathbf{Z}) \propto L(\boldsymbol{\theta}, \boldsymbol{\delta}, \sigma_\epsilon^2 | \mathbf{Z})^{\gamma_t} \pi(\boldsymbol{\theta}) \pi(\boldsymbol{\delta}) \pi(\sigma_\epsilon^2), \quad (\text{A7})$$

81 where γ_t 's are determined according to a schedule where $\gamma_0 = 0 < \gamma_1 < \dots < \gamma_T = 1$. For
 82 each $\tilde{\pi}_t(\boldsymbol{\theta}, \boldsymbol{\delta}, \sigma_\epsilon^2 | \mathbf{Z})$, the likelihood component is a fractional power of the original likelihood
 83 $L(\boldsymbol{\theta}, \boldsymbol{\delta}, \sigma_\epsilon^2 | \mathbf{Z})$. Using an adaptive incorporation schedule (Lee et al., 2020), we can select the
 84 appropriate $\boldsymbol{\gamma} = \{\gamma_0, \gamma_1, \dots, \gamma_T\}$ within the calibration algorithm.

85 For cycle $t = 1$, we set the importance distribution to be the prior distribution $p(\boldsymbol{\theta}, \boldsymbol{\delta}, \sigma_\epsilon^2) =$
 86 $p(\boldsymbol{\theta})p(\boldsymbol{\delta})p(\sigma_\epsilon^2)$, and the target distribution to be the first intermediate posterior distribution,
 87 $\pi_1(\boldsymbol{\theta}, \boldsymbol{\delta}, \sigma_\epsilon^2 | \mathbf{Z})$. For subsequent cycles t , the importance distribution is $\pi_{t-1}(\boldsymbol{\theta}, \boldsymbol{\delta}, \sigma_\epsilon^2 | \mathbf{Z})$ and
 88 the target distribution is $\pi_t(\boldsymbol{\theta}, \boldsymbol{\delta}, \sigma_\epsilon^2 | \mathbf{Z})$.

89 Next, we mutate the particles via short runs of the Metropolis-Hastings algorithm, where
 90 the stationary distribution is $\pi_t(\boldsymbol{\theta}, \boldsymbol{\delta}, \sigma_\epsilon^2 | \mathbf{Z})$, the t -th intermediate posterior distribution. Note
 91 that the importance and target distributions are consecutive (t -th and $(t+1)$ -th) intermediate
 92 posterior distributions, so there is considerable overlap between the high-probability regions
 93 of the two distributions. In the mutation stage, we employ the stopping rule from Lee et al.
 94 (2020) to control the number of Metropolis-Hastings updates; thereby preventing any unnec-
 95 essary computer model runs. The mutation stages ends when the Bhattacharyya distance
 96 (Bhattacharyya, 1946) between two sets of particles from the mutation stage stabilizes.

97 2.2 Adaptive incorporation schedule

98 To reduce computational costs and potentially reduce unnecessary computer model eval-
 99 uations, we adopt the adaptive incorporation schedule from Lee et al. (2020). For avoid
 100 confusion, we simplify the notation in this subsection by defining $\tilde{\boldsymbol{\theta}} = (\boldsymbol{\theta}, \sigma_\epsilon^2, \boldsymbol{\delta})$, the com-
 101 bined vector of unknown parameters. Upon initialization, we set the first incorporation
 102 increment $\gamma_0 = 0$. We draw the initial set of particles $\tilde{\boldsymbol{\theta}}_0$ from $\tilde{\pi}_0(\tilde{\boldsymbol{\theta}} | \mathbf{Z}) \propto L(\tilde{\boldsymbol{\theta}} | \mathbf{Z})^0 \pi(\tilde{\boldsymbol{\theta}}) = \pi(\tilde{\boldsymbol{\theta}})$,
 103 the prior distribution of model parameters. For the subsequent cycles $t = 1, 2, 3, \dots$, we

104 calculate the full likelihood $L(\tilde{\boldsymbol{\theta}}_{t-1}^{(i)}|\mathbf{Z})$ for $i = 1, \dots, N$ where $\tilde{\boldsymbol{\theta}}_{t-1}^{(i)}$ denotes the parameter samples from the previous cycle $t - 1$. Next, we compute the optimal γ_t that returns an effective sample size (ESS) of ESS_{thresh} or a sample size closest to ESS_{thresh} :
 105 $\gamma_t = \operatorname{argmin}_{\gamma} \{(ESS_{\gamma} - ESS_{thresh})^2\}$, where $\gamma \in (\gamma_{min}, 1 - \gamma_{t-1})$, γ_{min} is a previously set
 106 minimum incorporation value, $ESS_{\gamma_t} = \sum_{i=1}^N 1/w_t(\tilde{\boldsymbol{\theta}}_t^{(i)})^2$, and $w_t(\tilde{\boldsymbol{\theta}}_t^{(i)}) \propto L(\tilde{\boldsymbol{\theta}}_t^{(i)}|\mathbf{Z})^{\gamma}$. Note
 107 that we can lower computational costs by evaluating the full likelihood $L(\tilde{\boldsymbol{\theta}}_t^{(i)}|\mathbf{Z})$ only once
 108 before the optimization.

109 We stop the scheduling algorithm when $\sum_{i=1}^t \gamma_t = 1$, or when the entire likelihood has
 110 been incorporated and the target distribution evolves to the full posterior distribution $\tilde{\pi}(\tilde{\boldsymbol{\theta}}|\mathbf{Z})$.
 111 Note at each cycle t , we set the incorporation increment (γ_t) to be between γ_{min} and $1 -$
 112 $\sum_{i=1}^t \gamma_t$. The user will typically set the minimum incorporation increment γ_{min} and the
 113 threshold effective sample size, ESS_{thresh} . We provide our choice of γ_{min} and ESS_{thresh} in
 114 the next section (Implementation Details).

117 Adaptive likelihood incorporation schedule

118 1. Initialization: At $t = 0$, set $\gamma_0 = 0$.

119 2. When $t > 0$ and $\sum_{i=1}^{t-1} \gamma_i < 1$

- 120 • Compute $L(\tilde{\boldsymbol{\theta}}_{t-1}^{(i)}|\mathbf{Z})$ for $i = 1, \dots, N$
- 121 • Set $\gamma_t = \operatorname{argmin}_{\gamma} \{(ESS_{\gamma} - ESS_{thresh})^2\}$, where $ESS_{\gamma} = \sum_{i=1}^N \frac{1}{w_t^{(i)2}}$, $w_t^{(i)} \propto$
 122 $L(\tilde{\boldsymbol{\theta}}_t^{(i)}|\mathbf{Z})^{\gamma}$, and $\gamma \in (\gamma_{min}, 1 - \gamma_{t-1})$.
- 123 • Update $t \leftarrow t + 1$

124 3. When $\sum_{i=1}^{t-1} \gamma_i = 1$: Stop Calibration

125 2.3 HL-RDHM Calibration: Implementation Details

We now return to the original notation of the unknown parameters $\boldsymbol{\theta}$, σ_{δ}^2 , and σ_{ϵ}^2 . The target distribution is the full posterior distribution $\tilde{\pi}(\boldsymbol{\theta}, \sigma_{\delta}^2, \sigma_{\epsilon}^2|\mathbf{Z})$ and the Bayesian hierarchical framework for the HL-RDHM distributed hydrological model calibration is as follows:

$$\text{Data Model: } \quad \mathbf{Z}|\mathbf{Y}(\cdot), \boldsymbol{\theta}, \boldsymbol{\delta}, \sigma_{\epsilon}^2 \sim \mathcal{N}(\mathbf{Y}(\boldsymbol{\theta}) + \boldsymbol{\delta}, \sigma_{\epsilon}^2 \mathcal{I}) \quad (\text{A8})$$

$$\text{Process Model: } \quad \boldsymbol{\delta}|\sigma_{\delta}^2 \sim \mathcal{N}(\mathbf{0}, \sigma_{\delta}^2 \mathcal{I}) \quad (\text{A9})$$

$$\text{Parameter Model: } \quad \boldsymbol{\theta} \sim \pi(\boldsymbol{\theta}), \quad \sigma_{\delta}^2 \sim \pi(\sigma_{\delta}^2), \quad \sigma_{\epsilon}^2 \sim \pi(\sigma_{\epsilon}^2) \quad (\text{A10})$$

126 where $\pi(\boldsymbol{\theta})$, $\pi(\sigma_{\delta}^2)$, and $\pi(\sigma_{\epsilon}^2)$ denote the prior distributions of $\boldsymbol{\theta}$, σ_{δ}^2 , and σ_{ϵ}^2 , respectively.
 127 For $\pi(\boldsymbol{\theta})$, we place a priori independent uniform priors on each of the model parameters with
 128 ranges (lower and upper bounds) based on domain-area expertise.

129 Instead of estimating the nuisance parameters σ_{δ}^2 and σ_{ϵ}^2 separately, we chose to combine
 130 these as $\sigma^2 = \sigma_{\delta}^2 + \sigma_{\epsilon}^2$. We place a standard non-informative inverse gamma prior on the
 131 combined error variance $\sigma_{\epsilon}^2 \sim IG(0.2, 0.2)$. Note that we assume conditional independence

Algorithm 1: Fast Particle-based Calibration

Data: Z

Initialization:

Draw $\tilde{\theta}_0^{(i)} \sim p(\tilde{\theta})$ for particles $i = 1, \dots, N$.

Set $w_0^{(i)} = 1/N$, $\gamma_0 = 0$, and K ;

for cycles $t = 1, \dots, T$ **do**

1. Compute full likelihood:

 Calculate $L(\tilde{\theta}_{t-1}^{(i)} | \mathbf{Z})$ for $i = 1, \dots, N$;

2. Select optimal likelihood incorporation increment γ_t :

 Set $\gamma_t = \operatorname{argmin}_\gamma \{(ESS_{\gamma_t} - ESS_{thresh})^2\}$, where $\gamma \in (0.1, 1 - \sum_{h=1}^{t-1} \gamma_h)$

 Note: $ESS_{\gamma_t} = \sum_{i=1}^N \frac{1}{w_t^{(i)2}}$ and $w_t^{(i)} \propto L(\tilde{\theta}_t^{(i)} | \mathbf{Z})^{\gamma_t}$;

3. Compute importance weights:

$w_t^{(i)} \propto w_{t-1}^{(i)} \times L(\tilde{\theta}_t^{(i)} | \mathbf{Z})^{\gamma_t}$;

4. Re-sample particles via multinomial sampling:

 Draw $\tilde{\theta}_t^{(i)}$ from $\{\tilde{\theta}_{t-1}^{(1)}, \dots, \tilde{\theta}_{t-1}^{(N)}\}$ with probabilities $\propto \{w_t^{(1)}, \dots, w_t^{(N)}\}$;

5. Set intermediate posterior distribution:

 Set $\pi_t(\tilde{\theta} | \mathbf{Z}) \propto L(\tilde{\theta}_t | \mathbf{Z})^{\tilde{\gamma}} \pi(\tilde{\theta})$, where $\tilde{\gamma} = \sum_{j=1}^t \gamma_j$;

6. Mutation:

 Using each particle $(\tilde{\theta}_t^{(1)}, \dots, \tilde{\theta}_t^{(N)})$ as the initial value, run N chains of an MCMC algorithm with target distribution $\pi_t(\tilde{\theta} | \mathbf{Z})$ for $2K$ iterations

7. Check stopping criterion:

 Compute $\delta_B = D_B(h(\tilde{\theta}_t^K), h(\tilde{\theta}_t^{2K}))$;

if $\delta_B < \epsilon_B$ **then**

 | Set $\tilde{\theta}_t^{(i)} = \tilde{\theta}_t^{(i), 2K}$;

else

 | Run K additional updates and re-evaluate stopping criterion

 | Continue until stopping criterion is met

8. Stop when full likelihood is incorporated;

if $\sum_{i=1}^N \gamma_t = 1$ **then**

 | End Algorithm;

else

 | **Reset weights:** $w_t^{(i)} = 1/N$ for particles $i = 1, \dots, N$;

 | Set $t=t+1$ and return to Step 1;

132 among the extreme observations given the model outputs. The updated Bayesian hierarchical
 133 framework is:

$$\text{Data Model: } \mathbf{Z}|\mathbf{Y}(\cdot), \boldsymbol{\theta}, \sigma^2 \sim \mathcal{N}(\mathbf{Y}(\boldsymbol{\theta}), \sigma^2 \mathbf{I}) \quad (\text{A11})$$

$$\text{Parameter Model: } \boldsymbol{\theta} \sim \pi(\boldsymbol{\theta}), \quad \sigma^2 \sim \pi(\sigma^2) \quad (\text{A12})$$

134 While much of the fast particle-based approach is automated, the user must select the:
 135 (1) total number of particles, N ; (2) baseline number of Metropolis-Hastings updates run
 136 before checking the stopping criterion, K ; (3) minimum incorporation γ_{min} at each cycle;
 137 and (4) the effective sample size threshold ESS_{thresh} . We chose $N = 2015$ particles based
 138 on the available resources. On the Cheyenne HPC, this requires 56 nodes with 36 processors
 139 per node. For the stopping criterion, we use $K = 7$ as the baseline length. The floor
 140 for the incorporation increment is fixed at $\gamma_{min} = 0.1$ such that we incorporate at least
 141 $L(\boldsymbol{\theta}|\mathbf{Z})^{0.1}$ into the intermediate posterior at each cycle. Finally, the $ESS_{thresh} = N/2$, which
 142 is the typical threshold that activates resampling in many sequential Monte Carlo methods
 143 (Del Moral et al., 2006). We calibrate the HL-RDHM distributed hydrological model using
 144 Cheyenne (Computational and Information Systems Laboratory, 2017), a 5.34-petaflops high
 145 performance computer operated by the National Center for Atmospheric Research (NCAR).
 146 We employ message passing interface (MPI) and the R package `Rmpi` for any parallelized
 147 operations such as computing importance weights and particle mutation.

148 Consider the vector of HL-RDHM model parameters $\boldsymbol{\theta} = (\theta_1, \dots, \theta_{12})'$. The prior distribu-
 149 tion $\pi(\theta_j)$ for the j -th model parameters follow a univariate uniform distribution with lower
 150 and upper bounds specified by our hydrological model experts. $\theta_j \sim Unif(l_j, u_j)$ with hy-
 151 perparameters l_j (lower bound) and u_j (upper bound) specified in Table S1. We place a stan-
 152 dard non-informative inverse gamma prior on the combined error variance $\sigma^2 \sim IG(\alpha_{\sigma^2}, \beta_{\sigma^2})$
 153 where $\alpha_{\sigma^2} = 0.2$ and $\beta_{\sigma^2} = 0.2$.

References

- 154
- 155 Bayarri, M., Berger, J., Cafeo, J., Garcia-Donato, G., Liu, F., Palomo, J., Parthasarathy, R.,
156 Paulo, R., Sacks, J., Walsh, D., et al. (2007). Computer model validation with functional
157 output. *The Annals of Statistics*, 35(5):1874–1906.
- 158 Bhat, K. S., Haran, M., Goes, M., and Chen, M. (2010). Computer model calibration with
159 multivariate spatial output: A case study. *Frontiers of Statistical Decision Making and*
160 *Bayesian Analysis*, pages 168–184.
- 161 Bhattacharyya, A. (1946). On a measure of divergence between two multinomial populations.
162 *Sankhyā: The Indian Journal of Statistics*, pages 401–406.
- 163 Brynjarsdottir, J. and O’Hagan, A. (2014). Learning about physical parameters: The im-
164 portance of model discrepancy. *Inverse Problems*, 30(11):114007.
- 165 Chopin, N. (2002). A sequential particle filter method for static models. *Biometrika*,
166 89(3):539–552.
- 167 Computational and Information Systems Laboratory (2017). Cheyenne: HPE/SGI ICE XA
168 System (University Community Computing). Boulder, CO: National Center for Atmo-
169 spheric Research. doi:10.5065/D6RX99HX.
- 170 Crisan, D. and Doucet, A. (2000). Convergence of sequential Monte Carlo methods. *Signal*
171 *Processing Group, Department of Engineering, University of Cambridge, Technical Report*
172 *CUED/F-INFENG/TR381*, 1.
- 173 Del Moral, P., Doucet, A., and Jasra, A. (2006). Sequential Monte Carlo samplers. *Journal*
174 *of the Royal Statistical Society: Series B*, 68(3):411–436.
- 175 Doucet, A., De Freitas, N., and Gordon, N. (2001). An introduction to sequential Monte
176 Carlo methods. In *Sequential Monte Carlo Methods in Practice*, pages 3–14. Springer.
- 177 Doucet, A., Godsill, S., and Andrieu, C. (2000). On sequential Monte Carlo sampling
178 methods for Bayesian filtering. *Statistics and Computing*, 10(3):197–208.
- 179 Gilks, W. R. and Berzuini, C. (2001). Following a moving target—Monte Carlo inference for
180 dynamic Bayesian models. *Journal of the Royal Statistical Society: Series B (Statistical*
181 *Methodology)*, 63(1):127–146.
- 182 Gordon, N. J., Salmond, D. J., and Smith, A. F. (1993). Novel approach to nonlinear/non-
183 Gaussian Bayesian state estimation. In *IEE Proceedings F-radar and Signal Processing*,
184 volume 140, pages 107–113. IET.
- 185 Lee, B. S., Haran, M., Fuller, R. W., Pollard, D., and Keller, K. (2020). A fast particle-based
186 approach for calibrating a 3-d model of the antarctic ice sheet. *The Annals of Applied*
187 *Statistics*, 14(2):605–634.

- 188 Li, T., Sun, S., Sattar, T. P., and Corchado, J. M. (2014). Fight sample degeneracy and
189 impoverishment in particle filters: A review of intelligent approaches. *Expert Systems with*
190 *Applications*, 41(8):3944–3954.
- 191 Liang, F. and Wong, W. H. (2001). Real-Parameter Evolutionary Monte Carlo with ap-
192 plications to Bayesian mixture models. *Journal of the American Statistical Association*,
193 96(454):653–666.
- 194 Liu, J. and West, M. (2001). Combined parameter and state estimation in simulation-based
195 filtering. In *Sequential Monte Carlo Methods in Practice*, pages 197–223. Springer.
- 196 Murray, L. M., Lee, A., and Jacob, P. E. (2016). Parallel resampling in the particle filter.
197 *Journal of Computational and Graphical Statistics*, 25(3):789–805.
- 198 Neal, R. M. (2001). Annealed importance sampling. *Statistics and Computing*, 11(2):125–
199 139.
- 200 Papaioannou, I., Papadimitriou, C., and Straub, D. (2016). Sequential importance sampling
201 for structural reliability analysis. *Structural Safety*, 62:66–75.
- 202 Zhu, G., Li, X., Ma, J., Wang, Y., Liu, S., Huang, C., Zhang, K., and Hu, X. (2018). A new
203 moving strategy for the sequential Monte Carlo approach in optimizing the hydrological
204 model parameters. *Advances in Water Resources*, 114:164–179.

References

- Alfieri, L., Bisselink, B., Dottori, F., Naumann, G., de Roo, A., Salamon, P., et al. (2017). Global projections of river flood risk in a warmer world. *Earth's Future*.
<https://doi.org/10.1002/2016ef000485>
- Anderson, R. M., Koren, V. I., & Reed, S. M. (2006). Using SSURGO data to improve Sacramento Model a priori parameter estimates. *Journal of Hydrology*, 320(1), 103–116.
- Asher, M. J., Croke, B. F. W., Jakeman, A. J., & Peeters, L. J. M. (2015). A review of surrogate models and their application to groundwater modeling. *Water Resources Research*.
<https://doi.org/10.1002/2015wr016967>
- Ashley, S. T., & Ashley, W. S. (2008). Flood Fatalities in the United States. *Journal of Applied Meteorology and Climatology*, 47(3), 805–818.
- Bain, A., & Crisan, D. (2008). *Fundamentals of Stochastic Filtering*. Springer Science & Business Media.
- Bates, P. D., Quinn, N., Sampson, C., Smith, A., Wing, O., Sosa, J., et al. (2021). Combined modeling of US fluvial, pluvial, and coastal flood hazard under current and future climates. *Water Resources Research*, 57(2). <https://doi.org/10.1029/2020wr028673>
- Bayarri, M. J., Berger, J. O., Paulo, R., Sacks, J., Cafeo, J. A., Cavendish, J., et al. (2007a). A Framework for Validation of Computer Models. *Technometrics: A Journal of Statistics for the Physical, Chemical, and Engineering Sciences*, 49(2), 138–154.
- Bayarri, M. J., Walsh, D., Berger, J. O., Cafeo, J., Garcia-Donato, G., Liu, F., et al. (2007b). Computer model validation with functional output. *The Annals of Statistics*, 35(5), 1874–1906.
- Beven, K. J., and A. M. Binley, The future of distributed models: Model calibration and

- uncertainty prediction, *Hydrol. Processes*, 6, 279–298, 1992.
- Beven, K. (2014). The GLUE Methodology for Model Calibration with Uncertainty. *Applied Uncertainty Analysis for Flood Risk Management*.
https://doi.org/10.1142/9781848162716_0006
- Bhat, K. S., Haran, M., Goes, M., & Chen, M. (2010). Computer model calibration with multivariate spatial output: A case study. *Frontiers of Statistical Decision Making and Bayesian Analysis*, 168–184.
- Bhattacharyya, A. (1946). On a Measure of Divergence between Two Multinomial Populations. *Journal of the Indian Society of Agricultural Statistics. Indian Society of Agricultural Statistics*, 7(4), 401–406.
- Bitew, M. M., & Gebremichael, M. (2011). Evaluation of satellite rainfall products through hydrologic simulation in a fully distributed hydrologic model. *Water Resources Research*, 47(6). <https://doi.org/10.1029/2010wr009917>
- Blasone, R.-S., J. A. Vrugt, H. Madsen, D. Rosbjerg, B. A. Robinson, and G. A. Zyvoloski (2008a), Generalized likelihood uncertainty estimation (GLUE) using adaptive Markov chain Monte Carlo sampling, *Adv. Water Resour.*, 31, 630–648.
- Boulangé, J., Hanasaki, N., Yamazaki, D., & Pokhrel, Y. (2021). Role of dams in reducing global flood exposure under climate change. *Nature Communications*, 12(1), 417.
- Bowman, A. L., Franz, K. J., & Hogue, T. S. (2017). Case Studies of a MODIS-Based Potential Evapotranspiration Input to the Sacramento Soil Moisture Accounting Model. *Journal of Hydrometeorology*, 18(1), 151–158.
- Braak, C. J. F. T. (2006). A Markov Chain Monte Carlo version of the genetic algorithm Differential Evolution: easy Bayesian computing for real parameter spaces. *Statistics and*

Computing, 16(3), 239–249.

- Brunner, G. W. (1995). *HEC-RAS River Analysis System. Hydraulic Reference Manual. Version 1.0*. Hydrologic Engineering Center Davis CA. Retrieved from <https://apps.dtic.mil/sti/citations/ADA311952>
- Brynjarsdóttir, J., & O’Hagan, A. (2014). Learning about physical parameters: the importance of model discrepancy. *Inverse Problems*, 30(11), 114007.
- Carlberg, B., Franz, K., & Gallus, W. (2020). A Method to Account for QPF Spatial Displacement Errors in Short-Term Ensemble Streamflow Forecasting. *WATER*, 12(12), 3505.
- Chang, W., Haran, M., Olson, R., & Keller, K. (2014). Fast dimension-reduced climate model calibration and the effect of data aggregation. *The Annals of Applied Statistics*, 8(2), 649–673.
- Chang, W., Haran, M., Applegate, P., & Pollard, D. (2016). Calibrating an Ice Sheet Model Using High-Dimensional Binary Spatial Data. *Journal of the American Statistical Association*, 111(513), 57–72.
- Chester, M. V., Shane Underwood, B., & Samaras, C. (2020). Keeping infrastructure reliable under climate uncertainty. *Nature Climate Change*. <https://doi.org/10.1038/s41558-020-0741-0>
- Chopin, N. (2002). A sequential particle filter method for static models. *Biometrika*, 89(3), 539–552.
- Computational and Information Systems Laboratory (2017). Cheyenne: HPE/SGI ICE XA System (University Community Computing). Boulder, CO: National Center for Atmospheric Research. doi:10.5065/D6RX99HX.

- Constantine, P. G., Dow, E., & Wang, Q. (2014). Active Subspace Methods in Theory and Practice: Applications to Kriging Surfaces. *SIAM Journal on Scientific Computing*.
<https://doi.org/10.1137/130916138>
- Coulthard, T. J., Neal, J. C., Bates, P. D., Ramirez, J., de Almeida, G. A. M., & Hancock, G. R. (2013). Integrating the LISFLOOD-FP 2D hydrodynamic model with the CAESAR model: implications for modelling landscape evolution. *Earth Surface Processes and Landforms*, 38(15), 1897–1906.
- Craig, P. S., Goldstein, M., Seheult, A. H., & Smith, J. A. (1997). Pressure Matching for Hydrocarbon Reservoirs: A Case Study in the Use of Bayes Linear Strategies for Large Computer Experiments. In *Case Studies in Bayesian Statistics* (pp. 37–93). Springer New York.
- Crisan, D., & Doucet, A. (2000). Convergence of sequential Monte Carlo methods. *Signal Processing Group, Department of Engineering, University of Cambridge, Technical Report CUEDIF-INFENGrrR38, 1*. Retrieved from
<http://citeseerx.ist.psu.edu/viewdoc/download?doi=10.1.1.361.3193&rep=rep1&type=pdf>
- Davis and Skaggs. (1992). *Catalog of Residential Depth-Damage Functions Used by the Army Corps of Engineers in Flood Damage Estimation*. Retrieved from
<https://apps.dtic.mil/dtic/tr/fulltext/u2/a255462.pdf>
- Del Moral, P., Doucet, A., & Jasra, A. (2006). Sequential Monte Carlo samplers. *Journal of the Royal Statistical Society: Series B*, 68(3):411– 436.
- Didier, D., Baudry, J., Bernatchez, P., Dumont, D., Sadegh, M., Bismuth, E., et al. (2019). Multihazard simulation for coastal flood mapping: Bathtub versus numerical modelling in an open estuary, Eastern Canada. *Journal of Flood Risk Management*, 12(S1), e12505.

- Doucet, A., Godsill, S., & Andrieu, C. (2000). *Statistics and Computing*, 10(3), 197–208.
- Doucet, A., de Freitas, N., & Gordon, N. (2001). An Introduction to Sequential Monte Carlo Methods. In A. Doucet, N. de Freitas, & N. Gordon (Eds.), *Sequential Monte Carlo Methods in Practice* (pp. 3–14). New York, NY: Springer New York.
- Duan, Q., S. Sorooshian, and V. K. Gupta (1992), Effective and efficient global optimization for conceptual rainfall-runoff models, *Water Resour. Res.*, 28(4), 1015–1031, doi:10.1029/91WR02985.
- Edwards, N. R., Cameron, D., & Rougier, J. (2011). Precalibrating an intermediate complexity climate model. *Climate Dynamics*, 37(7-8), 1469–1482.
- Fares, A., Awal, R., Michaud, J., Chu, P.-S., Fares, S., Kodama, K., & Rosener, M. (2014). Rainfall-runoff modeling in a flashy tropical watershed using the distributed HL-RDHM model. *Journal of Hydrology*, 519, 3436–3447.
- FEMA, 2019: Flood Insurance Rate Map (FIRM). Federal Emergency Management Agency, <https://www.fema.gov/flood-insurance-ratemap-firm>.
- Fereshtehpour, M., & Karamouz, M. (2018). DEM resolution effects on coastal flood vulnerability assessment: Deterministic and probabilistic approach. *Water Resources Research*, 54(7), 4965–4982.
- Fisher, R. A., & Koven, C. D. (2020). Perspectives on the future of land surface models and the challenges of representing complex terrestrial systems. *Journal of Advances in Modeling Earth Systems*, 12(4). <https://doi.org/10.1029/2018ms001453>
- Gilks, W. R., & Berzuini, C. (2001). Following a moving target-Monte Carlo inference for dynamic Bayesian models. *Journal of the Royal Statistical Society. Series B, Statistical Methodology*, 63(1), 127–146.

- Gomez, M., Sharma, S., Reed, S., & Mejia, A. (2019). Skill of ensemble flood inundation forecasts at short- to medium-range timescales. *Journal of Hydrology*, 568, 207–220.
- Goodman, J., & Weare, J. (2010). Ensemble samplers with affine invariance. *Communications in Applied Mathematics and Computational Science*, 5(1), 65–80.
- Gordon, N. J., Salmond, D. J., & Smith, A. F. M. (1993). Novel approach to nonlinear/non-Gaussian Bayesian state estimation. In *IEE Proceedings F-radar and signal processing* (Vol. 140, pp. 107–113). IET.
- Gou, J., Miao, C., Duan, Q., Tang, Q., Di, Z., Liao, W., et al. (2020). Sensitivity Analysis-Based Automatic Parameter Calibration of the VIC Model for Streamflow Simulations Over China. *Water Resources Research*. <https://doi.org/10.1029/2019wr025968>
- Gramacy, R. B. (2020). *Surrogates: Gaussian process modeling, design, and optimization for the applied sciences*. Chapman and Hall/CRC.
- Gramacy, R. B., & Apley, D. W. (2015). Local Gaussian Process Approximation for Large Computer Experiments. *Journal of Computational and Graphical Statistics: A Joint Publication of American Statistical Association, Institute of Mathematical Statistics, Interface Foundation of North America*, 24(2), 561–578.
- Gupta, H. V., S. Sorooshian, and P. O. Yapo (1998), Toward improved calibration of hydrologic models: Multiple and noncommensurable measures of information, *Water Resour. Res.*, 34(4), 751–763, doi:10.1029/97WR03495.
- Gupta, H. V., Clark, M. P., Vrugt, J. A., Abramowitz, G., & Ye, M. (2012). Towards a comprehensive assessment of model structural adequacy. *Water Resources Research*, 48(8). <https://doi.org/10.1029/2011WR011044>
- Helton, J. C., & Davis, F. J. (2003). Latin hypercube sampling and the propagation of uncertainty

- in analyses of complex systems. *Reliability Engineering & System Safety*, 81(1), 23–69.
- Herman, J. D., Reed, P. M., & Wagener, T. (2013). Time-varying sensitivity analysis clarifies the effects of watershed model formulation on model behavior. *Water Resources Research*, 49(3), 1400–1414.
- Higdon, D. (2003). for inference in computationally intensive inverse problems. In *Bayesian Statistics 7: Proceedings of the Seventh Valencia International Meeting* (p. 181). Oxford University Press.
- Higdon, D., Kennedy, M., Cavendish, J. C., Cafeo, J. A., & Ryne, R. D. (2004). Combining Field Data and Computer Simulations for Calibration and Prediction. *SIAM Journal of Scientific Computing*, 26(2), 448–466.
- Higdon, D., Gattiker, J., Williams, B., & Rightley, M. (2008). Computer Model Calibration Using High-Dimensional Output. *Journal of the American Statistical Association*, 103(482), 570–583.
- Holden, P. B., Edwards, N. R., Oliver, K. I. C., Lenton, T. M., & Wilkinson, R. D. (2010). A probabilistic calibration of climate sensitivity and terrestrial carbon change in GENIE-1. *Climate Dynamics*, 35(5), 785–806.
- Homer, C., Dewitz, J., Yang, L., Jin, S., Danielson, P., Xian, G., et al. (2015). Completion of the 2011 National Land Cover Database for the conterminous United States--representing a decade of land cover change information. *Photogrammetric Engineering & Remote Sensing*, 81(5), 345–354.
- Hsu, K.-L., Moradkhani, H., & Sorooshian, S. (2009). A sequential Bayesian approach for hydrologic model selection and prediction. *Water Resources Research*, 45(12).
<https://doi.org/10.1029/2008wr006824>

- Hu, J., Chen, S., Behrangi, A., & Yuan, H. (2019). Parametric uncertainty assessment in hydrological modeling using the generalized polynomial chaos expansion. *Journal of Hydrology*, 579, 124158.
- Hwang, J. T., & Martins, J. R. R. A. (2018). A fast-prediction surrogate model for large datasets. *Aerospace Science and Technology*, 75, 74–87.
- Jeremiah, E., Sisson, S., Marshall, L., Mehrotra, R., & Sharma, A. (2011). Bayesian calibration and uncertainty analysis of hydrological models: A comparison of adaptive Metropolis and sequential Monte Carlo samplers. *Water Resources Research*, 47(7).
<https://doi.org/10.1029/2010wr010217>
- Judi, D. R., Rakowski, C. L., Waichler, S. R., Feng, Y., & Wigmosta, M. S. (2018). Integrated Modeling Approach for the Development of Climate-Informed, Actionable Information. *WATER*, 10(6), 775.
- Kalyanaraman, J., Kawajiri, Y., Lively, R. P., & Realff, M. J. (2016). Uncertainty quantification via bayesian inference using sequential monte carlo methods for CO₂adsorption process. *AIChE Journal*. <https://doi.org/10.1002/aic.15381>
- Kamali, B., Mousavi, S. J., & Abbaspour, K. C. (2013). Automatic calibration of HEC-HMS using single-objective and multi-objective PSO algorithms. *Hydrological Processes*, 27(26), 4028–4042.
- Kantas, N., Beskos, A., & Jasra, A. (2014). Sequential Monte Carlo Methods for High-Dimensional Inverse Problems: A Case Study for the Navier--Stokes Equations. *SIAM/ASA Journal on Uncertainty Quantification*, 2(1), 464–489.
- Kavetski, D., Kuczera, G., & Franks, S. W. (2006). Bayesian analysis of input uncertainty in hydrological modeling: 2. Application. *Water resources research*, 42(3).

10.1029/2005WR004376

- Kavetski, D., Fenicia, F., Reichert, P., & Albert, C. (2018). Signature-Domain Calibration of Hydrological Models Using Approximate Bayesian Computation: Theory and Comparison to Existing Applications. *Water Resources Research*. <https://doi.org/10.1002/2017wr020528>
- Kennedy, M. C., & O'Hagan, A. (2001). Bayesian calibration of computer models. *Journal of the Royal Statistical Society. Series B, Statistical Methodology*, 63(3), 425–464.
- Kim S, Shen H, Noh S, Seo DJ, Philips B (2021) High-resolution modeling and prediction of urban floods using WRF-Hydro and data assimilation. *J Hydrol* 598:1–14
- Knutti, R., T. F. Stocker, F. Joos, and G.-K. Plattner (2002), Constraints on radiative forcing and future climate change from observations and climate model ensembles, *Nature*, 416, 719–723.
- Koren, V., Reed, S., Smith, M., Zhang, Z., & Seo, D.-J. (2004). Hydrology laboratory research modeling system (HL-RMS) of the US national weather service. *Journal of Hydrology*, 291(3), 297–318.
- Kuzmin, V., Seo, D.-J., & Koren, V. (2008). Fast and efficient optimization of hydrologic model parameters using a priori estimates and stepwise line search. *Journal of Hydrology*, 353(1), 109–128.
- Lahmers, T. M., Hazenberg, P., Gupta, H., Castro, C., Gochis, D., Dugger, A., et al. (2021). Evaluation of NOAA National Water Model Parameter Calibration in Semiarid Environments Prone to Channel Infiltration. *Journal of Hydrometeorology*, 22(11), 2939–2969.
- Lataniotis, C., Marelli, S., & Sudret, B. (2020). EXTENDING CLASSICAL SURROGATE MODELING TO HIGH DIMENSIONS THROUGH SUPERVISED DIMENSIONALITY

- REDUCTION: A DATA-DRIVEN APPROACH. *International Journal for Uncertainty Quantification*, 10(1). <https://doi.org/10.1615/Int.J.UncertaintyQuantification.2020031935>
- Laloy, E., & Vrugt, J. A. (2012). High-dimensional posterior exploration of hydrologic models using multiple-try DREAM(ZS) and high-performance computing. *Water Resources Research*, 48, W01526. <https://doi.org/10.1029/2011WR010608>
- Lee, B. S., Haran, M., Fuller, R. W., Pollard, D., & Keller, K. (2020). A fast particle-based approach for calibrating a 3-D model of the Antarctic ice sheet. *The Annals of Applied Statistics*, 14(2), 605–634.
- Lempert, R. J. (2002). A new decision sciences for complex systems. *Proceedings of the National Academy of Sciences of the United States of America*, 99 Suppl 3, 7309–7313.
- Li, T., Sun, S., Sattar, T. P., & Corchado, J. M. (2014). Fight sample degeneracy and impoverishment in particle filters: A review of intelligent approaches. *Expert Systems with Applications*, 41(8), 3944–3954.
- Liang, F., & Wong, W. H. (2001). Real-Parameter Evolutionary Monte Carlo With Applications to Bayesian Mixture Models. *Journal of the American Statistical Association*, 96(454), 653–666.
- Liu, J., & West, M. (2001). Combined Parameter and State Estimation in Simulation-Based Filtering. In A. Doucet, N. de Freitas, & N. Gordon (Eds.), *Sequential Monte Carlo Methods in Practice* (pp. 197–223). New York, NY: Springer New York.
- Liu, J. S., Liang, F., & Wong, W. H. (2000). The Multiple-Try Method and Local Optimization in Metropolis Sampling. *Journal of the American Statistical Association*, 95(449), 121–134.
- Liu, X., & Guillas, S. (2017). Dimension Reduction for Gaussian Process Emulation: An Application to the Influence of Bathymetry on Tsunami Heights. *SIAM/ASA Journal on*

Uncertainty Quantification, 5(1), 787–812.

- Liu, Y., Hejazi, M., Li, H., Zhang, X., & Leng, G. (2018). A hydrological emulator for global applications – HE v1.0.0. *Geoscientific Model Development*. <https://doi.org/10.5194/gmd-11-1077-2018>
- Liu, Z., & Merwade, V. (2018). Accounting for model structure, parameter and input forcing uncertainty in flood inundation modeling using Bayesian model averaging. *Journal of Hydrology*, 565, 138–149.
- Mak, S., Sung, C.-L., Wang, X., Yeh, S.-T., Chang, Y.-H., Joseph, V. R., et al. (2018). An Efficient Surrogate Model for Emulation and Physics Extraction of Large Eddy Simulations. *Journal of the American Statistical Association*, 113(524), 1443–1456.
- Mason, S. J., & Graham, N. E. (2002). Areas beneath the relative operating characteristics (ROC) and relative operating levels (ROL) curves: Statistical significance and interpretation. *Quarterly Journal of the Royal Meteorological Society*, 128(584), 2145–2166.
- Mckay, M. D., Beckman, R. J., & Conover, W. J. (2000). A Comparison of Three Methods for Selecting Values of Input Variables in the Analysis of Output From a Computer Code. *Technometrics: A Journal of Statistics for the Physical, Chemical, and Engineering Sciences*, 42(1), 55–61.
- McEnery, J., Ingram, J., Duan, Q., Adams, T., & Anderson, L. (2005). NOAA'S ADVANCED HYDROLOGIC PREDICTION SERVICE: Building Pathways for Better Science in Water Forecasting. *Bulletin of the American Meteorological Society*, 86(3), 375–386.
- Mejia, A. I., & Reed, S. M. (2011). Evaluating the effects of parameterized cross section shapes and simplified routing with a coupled distributed hydrologic and hydraulic model. *Journal*

of Hydrology, 409(1), 512–524.

Melsen, L., Teuling, A., Torfs, P., Zappa, M., Mizukami, N., Mendoza, P., Clark, M. P., &

Uijlenhoet, R. (2019). Subjective modeling decisions can significantly impact the

simulation of flood and drought events. *Journal of Hydrology*, 568, 1093–1104.

Mendoza, P. A., Clark, M. P., Mizukami, N., Newman, A. J., Barlage, M., Gutmann, E. D., et al.

(2015). Effects of Hydrologic Model Choice and Calibration on the Portrayal of Climate

Change Impacts. *Journal of Hydrometeorology*, 16(2), 762–780.

Merz, B., Hall, J., Disse, M., & Schumann, A. (2010). Fluvial flood risk management in a

changing world. *Natural Hazards and Earth System Sciences*, 10(3), 509–527.

Mizukami, N., Rakovec, O., Newman, A. J., Clark, M. P., Wood, A. W., Gupta, H. V., & Kumar,

R. (2019). On the choice of calibration metrics for “high-flow” estimation using hydrologic

models. *Hydrology and Earth System Sciences*, 23(6), 2601–2614.

Morzfeld, M., Day, M. S., Grout, R. W., Heng Pau, G. S., Finsterle, S. A., & Bell, J. B. (2018).

Iterative Importance Sampling Algorithms for Parameter Estimation. *SIAM Journal of*

Scientific Computing, 40(2), B329–B352.

Murphy, A. H. (1970). THE RANKED PROBABILITY SCORE AND THE PROBABILITY

SCORE: A COMPARISON. *Monthly Weather Review*, 98(12), 917–924.

Murphy, A. H. (1973). A New Vector Partition of the Probability Score. *Journal of Applied*

Meteorology and Climatology, 12(4), 595–600.

Murray, L. M., Lee, A., & Jacob, P. E. (2016). Parallel Resampling in the Particle Filter. *Journal*

of Computational and Graphical Statistics: A Joint Publication of American Statistical

Association, Institute of Mathematical Statistics, Interface Foundation of North America,

25(3), 789–805.

- Neal, R. M. (2001). Annealed importance sampling. *Statistics and Computing*, 11(2), 125–139.
- Neumann, T., & Ahrendt, K. (2013). Comparing The“ Bathtub Method” With Mike 21 Hd Flow Model For Modelling Storm Surge Inundation. *Ecologic Institute, Berlin, Germany*. Retrieved from https://edoc.sub.uni-hamburg.de/klimawandel/frontdoor/deliver/index/docId/835/file/RADOST_BATHTUB_034.pdf
- NWS, 2011: National Weather Service. Hydrology Laboratory-Research Distributed Hydrologic Model (HL-RDHM) user manual, version 3.2.0. NWS Rep., 131 pp.
- Oakley, J. E. (2009). Decision-Theoretic Sensitivity Analysis for Complex Computer Models. *Technometrics: A Journal of Statistics for the Physical, Chemical, and Engineering Sciences*, 51(2), 121–129.
- Papadimitriou, I., Papadimitriou, C., & Straub, D. (2016). Sequential importance sampling for structural reliability analysis. *Structural Safety*, 62, 66–75.
- Park, S., Hwang, J. P., Kim, E., & Kang, H.-J. (2009). A New Evolutionary Particle Filter for the Prevention of Sample Impoverishment. *IEEE Transactions on Evolutionary Computation*, 13(4), 801–809.
- Pianosi, F., Beven, K., Freer, J., Hall, J. W., Rougier, J., Stephenson, D. B., & Wagener, T. (2016). Sensitivity analysis of environmental models: A systematic review with practical workflow. *Environmental Modelling & Software*, 79, 214–232.
- Prat, O. P., & Nelson, B. R. (2015). Evaluation of precipitation estimates over CONUS derived from satellite, radar, and rain gauge data sets at daily to annual scales (2002–2012). *Hydrology and Earth System Sciences*. <https://doi.org/10.5194/hess-19-2037-2015>
- Rafieenasab, A., Norouzi, A., Kim, S., Habibi, H., Nazari, B., Seo, D.-J., et al. (2015). Toward

- high-resolution flash flood prediction in large urban areas – Analysis of sensitivity to spatiotemporal resolution of rainfall input and hydrologic modeling. *Journal of Hydrology*, *531*, 370–388.
- Raje, D., & Krishnan, R. (2012). Bayesian parameter uncertainty modeling in a macroscale hydrologic model and its impact on Indian river basin hydrology under climate change. *Water Resources Research*, *48*(8). <https://doi.org/10.1029/2011wr011123>
- Rajib, A., Liu, Z., Merwade, V., Tavakoly, A. A., & Follum, M. L. (2020). Towards a large-scale locally relevant flood inundation modeling framework using SWAT and LISFLOOD-FP. *Journal of Hydrology*, *581*, 124406.
- Razavi, S., & Tolson, B. A. (2013). An efficient framework for hydrologic model calibration on long data periods. *Water Resources Research*, *49*(12), 8418–8431.
- Read, L. K., & Vogel, R. M. (2015). Reliability, return periods, and risk under nonstationarity. *Water Resources Research*, *51*(8), 6381–6398.
- Reed, S., Schaake, J., & Zhang, Z. (2007). A distributed hydrologic model and threshold frequency-based method for flash flood forecasting at ungauged locations. *Journal of Hydrology*, *337*(3), 402–420.
- Reed, P. M., Hadjimichael, A., Malek, K., Karimi, T., Vernon, C. R., Srikrishnan, V., et al. (2022). Addressing Uncertainty in MultiSector Dynamics Research. Retrieved from <https://uc-ebook.org/>
- Rojas, M., Quintero, F., & Krajewski, W. F. (2020). Performance of the national water model in Iowa using independent observations. *Journal of the American Water Resources Association*, *56*(4), 568–585.
- Ruckert, K. L., Srikrishnan, V., & Keller, K. (2019). Characterizing the deep uncertainties

- surrounding coastal flood hazard projections: A case study for Norfolk, VA. *Scientific Reports*, 9(1), 11373.
- Sacks, J., Welch, W. J., Mitchell, T. J., & Wynn, H. P. (1989). Design and Analysis of Computer Experiments. *Schweizerische Monatsschrift Fur Zahnheilkunde = Revue Mensuelle Suisse D'odonto-Stomatologie / SSO*, 4(4), 409–423.
- Salas, F. R., Somos-Valenzuela, M. A., Dugger, A., Maidment, D. R., Gochis, D. J., David, C. H., et al. (2018a). Towards real-time continental scale streamflow simulation in continuous and discrete space. *Journal of the American Water Resources Association*, 54(1), 7–27.
- Salas, J. D., Obeysekera, J., & Vogel, R. M. (2018b). Techniques for assessing water infrastructure for nonstationary extreme events: a review. *Hydrological Sciences Journal*, 63(3), 325–352.
- Sanders, B. F., Schubert, J. E., Goodrich, K. A., Houston, D., Feldman, D. L., Basolo, V., et al. (2020). Collaborative Modeling With Fine-Resolution Data Enhances Flood Awareness, Minimizes Differences in Flood Perception, and Produces Actionable Flood Maps. *Earth's Future*. <https://doi.org/10.1029/2019ef001391>
- Scawthorn, C., Blais, N., Seligson, H., Tate, E., Mifflin, E., Thomas, W., et al. (2006). HAZUS-MH flood loss estimation methodology. I: Overview and flood hazard characterization. *Natural Hazards Review*, 7(2), 60–71.
- Shafii, M., Tolson, B., & Shawn Matott, L. (2015). Addressing subjective decision-making inherent in GLUE-based multi-criteria rainfall–runoff model calibration. *Journal of Hydrology*, 523, 693–705.
- Sharma, S., Siddique, R., Reed, S., Ahnert, P., & Mejia, A. (2019). Hydrological model diversity enhances streamflow forecast skill at short- to medium-range timescales. *Water Resources*

Research, 55(2), 1510–1530.

Sharma, S., Gomez, M., Keller, K., Nicholas, R., & Mejia, A. (2021). Regional Flood Risk Projections under Climate Change. *Journal of Hydrometeorology*, -1(aop).

<https://doi.org/10.1175/JHM-D-20-0238.1>

Siddique, R., & Mejia, A. (2017). Ensemble Streamflow Forecasting across the U.S. Mid-Atlantic Region with a Distributed Hydrological Model Forced by GEFS Reforecasts. *Journal of Hydrometeorology*, 18(7), 1905–1928.

Smith, T., Marshall, L., & Sharma, A. (2015). Modeling residual hydrologic errors with Bayesian inference. *Journal of Hydrology*, 528, 29-37.

Sorooshian, S., Q. Y. Duan, and V. K. Gupta (1993), Calibration of rainfall-runoff models—Application of global optimization to the Sacramento soil-moisture accounting model, *Water Resour. Res.*, 29(4), 1185–1194, doi:10.1029/92WR02617.

Stein, M. (1987). Large Sample Properties of Simulations Using Latin Hypercube Sampling. *Technometrics: A Journal of Statistics for the Physical, Chemical, and Engineering Sciences*, 29(2), 143–151.

Steinberg, D. M., & Lin, D. K. J. (2006). A construction method for orthogonal Latin hypercube designs. *Biometrika*. <https://doi.org/10.1093/biomet/93.2.279>

Stedinger, J. R., R. M. Vogel, S. U. Lee, and R. Batchelder (2008), Appraisal of the generalized likelihood uncertainty estimation (GLUE) method, *Water Resour. Res.*, 44, W00B06, doi:10.1029/2008WR006822.

Storn, R., & Price, K. (1997). *Journal of Global Optimization*, 11(4), 341–359.

Su, Y., Feng, Q., Zhu, G., Gu, C., Wang, Y., Shang, S., et al. (2018). A hierarchical Bayesian approach for multi-site optimization of a satellite-based evapotranspiration model.

Hydrological Processes, 32(26), 3907–3923.

- Tang, Y., Marshall, L., Sharma, A., & Smith, T. (2016). Tools for investigating the prior distribution in Bayesian hydrology. *Journal of Hydrology*, 538, 551-562.
- Tarawneh, E., Bridge, J., & Macdonald, N. (2016). A pre-calibration approach to select optimum inputs for hydrological models in data-scarce regions. *Hydrology and Earth System Sciences*. <https://doi.org/10.5194/hess-20-4391-2016>
- Tellman, B., Sullivan, J. A., Kuhn, C., Kettner, A. J., Doyle, C. S., Brakenridge, G. R., et al. (2021). Satellite imaging reveals increased proportion of population exposed to floods. *Nature*, 596(7870), 80–86.
- Vrugt, J. A., H. V. Gupta, W. Bouten, and S. Sorooshian (2003), A Shuffled Complex Evolution Metropolis algorithm for optimization and uncertainty assessment of hydrologic model parameters, *Water Resour. Res.*, 39(8), 1201, doi:10.1029/2002WR001642.
- Vrugt, J. A., C. J. F. ter Braak, C. G. H. Diks, B. A. Robinson, J. M. Hyman, and D. Higdon (2009), Accelerating Markov Chain Monte Carlo simulation by differential evolution with self-adaptive randomized subspace sampling, *Int. J. Nonlinear Sci. Numer. Simul.*, 10(3), 273–290.
- Vrugt, J. A., C. J. F. ter Braak, M. P. Clark, J. M. Hyman, and B. A. Robinson (2008), Treatment of input uncertainty in hydrologic modeling: Doing hydrology backward with Markov chain Monte Carlo simulation, *Water Resour. Res.*, 44, W00B09, doi:10.1029/2007WR006720.
- Wasko, C., Westra, S., Nathan, R., Orr, H. G., Villarini, G., Villalobos Herrera, R., & Fowler, H. J. (2021). Incorporating climate change in flood estimation guidance. *Philosophical Transactions. Series A, Mathematical, Physical, and Engineering Sciences*, 379(2195), 20190548.

- Wing, O. E. J., Bates, P. D., Smith, A. M., Sampson, C. C., Johnson, K. A., Fargione, J., & Morefield, P. (2018). Estimates of present and future flood risk in the conterminous United States. *Environmental Research Letters: ERL [Web Site]*, 13(3), 034023.
- Wing, O. E. J., Pinter, N., Bates, P. D., & Kousky, C. (2020). New insights into US flood vulnerability revealed from flood insurance big data. *Nature Communications*, 11(1), 1444.
- Winsemius, H. C., Jeroen C J, van Beek, L. P. H., Bierkens, M. F. P., Bouwman, A., Jongman, B., et al. (2015). Global drivers of future river flood risk. *Nature Climate Change*, 6(4), 381–385.
- Wong, T. E., & Keller, K. (2017). Deep Uncertainty Surrounding Coastal Flood Risk Projections: A Case Study for New Orleans. *Earth's Future*.
<https://doi.org/10.1002/2017ef000607>
- Yunus, A. P., Avtar, R., Kraines, S., Yamamuro, M., Lindberg, F., & Grimmond, C. S. B. (2016). Uncertainties in Tidally Adjusted Estimates of Sea Level Rise Flooding (Bathtub Model) for the Greater London. *Remote Sensing*, 8(5), 366.
- Zarekarizi, M., Srikrishnan, V., & Keller, K. (2020). Neglecting uncertainties biases house-elevation decisions to manage riverine flood risks. *Nature Communications*, 11(1), 5361.
- Zarzar, C. M., Hosseiny, H., Siddique, R., Gomez, M., Smith, V., Mejia, A., & Dyer, J. (2018). A hydraulic MultiModel ensemble framework for visualizing flood inundation uncertainty. *Journal of the American Water Resources Association*, 54(4), 807–819.
- Zhu, G., Li, X., Ma, J., Wang, Y., Liu, S., Huang, C., et al. (2018). A new moving strategy for the sequential Monte Carlo approach in optimizing the hydrological model parameters. *Advances in Water Resources*, 114, 164–179.